

Characterizing the Chemically-Enriched Circumgalactic Medium of ~ 38000 Luminous Red Galaxies in SDSS DR12

Yun-Hsin Huang^{1*}, Hsiao-Wen Chen^{1†}, Sean D. Johnson¹ and Benjamin J. Weiner²

¹*Department of Astronomy & Astrophysics, and Kavli Institute for Cosmological Physics, The University of Chicago, Chicago, IL 60637, USA*

²*Steward Observatory, University of Arizona, Tucson, AZ 85721, USA*

6 May 2019

ABSTRACT

We report a definitive detection of chemically-enriched cool gas around massive, quiescent galaxies at $z \approx 0.4 - 0.7$. The result is based on a survey of 37621 luminous red galaxy (LRG)-QSO pairs in SDSS DR12 with projected distance $d < 500$ kpc. The LRGs are characterized by a predominantly old (age $\gtrsim 1$ Gyr) stellar population with 13% displaying [O II] emission features and LINER-like spectra. Both passive and [O II]-emitting LRGs share the same stellar mass distribution with a mean of $\langle \log(M_*/M_\odot) \rangle \approx 11.4$ and a dispersion of 0.2 dex. Both LRG populations exhibit associated strong Mg II absorbers out to $d < 500$ kpc. The mean gas covering fraction at $d \lesssim 120$ kpc is $\langle \kappa \rangle_{\text{Mg II}} > 15\%$ and declines quickly to $\langle \kappa \rangle_{\text{Mg II}} \approx 5\%$ at $d \lesssim 500$ kpc. No clear dependence on stellar mass is detected for the observed Mg II absorption properties. The observed velocity dispersion of Mg II absorbing gas relative to either passive or [O II]-emitting LRGs is merely 60% of what is expected from virial motion in these massive halos. While no apparent azimuthal dependence is seen for $\langle \kappa \rangle_{\text{Mg II}}$ around passive LRGs at all radii, a modest enhancement in $\langle \kappa \rangle_{\text{Mg II}}$ is detected along the major axis of [O II]-emitting LRGs at $d < 50$ kpc. The suppressed velocity dispersion of Mg II absorbing gas around both passive and [O II]-emitting LRGs, together with an elevated $\langle \kappa \rangle_{\text{Mg II}}$ along the major axis of [O II]-emitting LRGs at $d < 50$ kpc, provides important insights into the origin of the observed chemically-enriched cool gas in LRG halos. We consider different scenarios and conclude that the observed Mg II absorbers around LRGs are best-explained by a combination of cool clouds formed in thermally unstable LRG halos and satellite accretion through filaments.

Key words: surveys – galaxies: haloes – galaxies: elliptical and lenticular, cD – quasars: absorption lines – galaxies: statistics

1 INTRODUCTION

Luminous red galaxies (LRGs) uncovered in the Sloan Digital Sky Survey (SDSS; York et al. 2000; Eisenstein et al. 2011) have luminosities of $\approx 5 L_*$ (e.g. Tojeiro et al. 2011) and reside in halos of $M_{\text{halo}} \gtrsim 10^{13} M_\odot$ (e.g., Blake et al. 2008; Zhu et al. 2014). These galaxies exhibit optical colors that resemble nearby elliptical galaxies with little on-going star formation (Eisenstein et al. 2001). The LRGs constitute a homogeneous sample of massive galaxies characterized by old stellar populations and provide an ideal laboratory for

studying galaxy formation and evolution at the high-mass end.

Mg II $\lambda\lambda$ 2793,2803 absorption features are commonly seen in the spectra of distant QSOs (e.g., Charlton et al. 2003). These absorbers originate in cool gas of temperature $T \sim 10^4$ K (e.g., Bergeron & Stasińska 1986) and neutral hydrogen column density ranging from $N(\text{HI}) \lesssim 10^{18} \text{ cm}^{-2}$ to $N(\text{HI}) \approx 10^{22} \text{ cm}^{-2}$ (e.g., Rao et al. 2006), and provide a sensitive probe of diffuse interstellar medium (ISM) and circumgalactic medium (CGM) along individual QSO sight-lines.

It has been well-established over the past two decades that typical L_* and sub- L_* galaxies are surrounded by extended Mg II absorbing gas out to projected distance of $d = 50 - 100$ kpc with a mean gas covering fraction of

* E-mail: yunhsin@uchicago.edu

† E-mail: hchen@oddjob.uchicago.edu

$\langle \kappa \rangle_{\text{Mg II}} \gtrsim 70\%$ (e.g., Bowen et al. 1995; Chen & Tinker 2008; Chen et al. 2010a)¹. The presence of chemically-enriched cool gas at ~ 100 kpc from star-forming regions can be explained by two competing models: infall (e.g., Mo & Miralda-Escudé 1996; Maller & Bullock 2004) and outflows (e.g., Weiner et al. 2009; Murray et al. 2011). Depending on the relative locations of the absorber and its associated galaxy, infalling gas and outflowing material can show similar line-of-sight velocity offset. In addition, depending on how efficiently chemical species are mixed in with surrounding medium, outflowing materials can appear as low-metallicity gas. Consequently, distinguishing between the two scenarios based on available empirical data remains challenging.

CGM studies focusing on halos around quiescent galaxies offer a promising avenue for resolving the ambiguous contributions between infall and outflows to the observed absorber statistics in the halos. The predominantly old stellar populations of quiescent galaxies, together with little/no on-going star formation, indicate a diminishing influence of young starburst driven winds on their halo gas. Mg II absorbers have been found to cluster strongly with LRGs, which suggests a non-negligible presence of these Mg II absorbers in these massive, quiescent halos (e.g., Gauthier et al. 2009; Lundgren et al. 2009; Zhu et al. 2014). Spectroscopic follow-up of close LRG-QSO pairs by Gauthier et al. (2010) and Gauthier & Chen (2011) further confirmed that indeed roughly $(14 \pm 6)\%$ of LRGs have associated Mg II absorbers at $d < 500$ kpc.

The non-negligible presence of chemically-enriched cool gas near LRGs extends the findings of HI gas in nearby elliptical galaxies (e.g., Oosterloo et al. 2010) to higher redshifts. These massive, quiescent galaxies provide an ideal laboratory for testing possible physical mechanisms to widely distribute heavy elements away from stars in the absence of starburst outflows. Likely scenarios include cold flows or filaments from the intergalactic medium (e.g., Kereš et al. 2009; Faucher-Giguère & Kereš 2011; Nelson et al. 2013), pressure-supported cool clouds in a hot halo (e.g., Mo & Miralda-Escudé 1996; Maller & Bullock 2004), and stripped materials from satellite galaxies (e.g., Agertz et al. 2009).

While some of these physical mechanisms provide a compelling explanation of the detected cool gas in hot halos, they remain hypothetical due to a lack of empirical constraints. To date, only a handful of galaxies have been studied in detail to probe the origin of their cool gas content. For example, Nestor et al. (2011) and Gauthier (2013) considered a small sample of LRGs with associated ultra-strong Mg II absorbers of $W_r(2796) \gtrsim 4 \text{ \AA}$, and found that these LRGs preferentially reside in a group environment. The presence of a galaxy group is qualitatively consistent with the

expectation of the observed Mg II absorbers originating in stripped gas in the intergroup medium.

As a first step toward a better understanding of the physical origin of chemically-enriched cool gas in massive quiescent halos, we make use of the vast spectroscopic data available in the public SDSS data archive to obtain refined measurements of the incidence and covering fraction of Mg II absorbing gas in LRG halos. As described below, our study is based on an unprecedentedly large sample of $\sim 38,000$ LRGs spectroscopically identified at projected distances of $d < 500$ kpc from the sightline of a background QSO. Both LRGs and the background QSOs are found in the SDSS spectroscopic catalog from DR12 (Alam et al. 2015). While the signal-to-noise (S/N) of the QSO spectra varies according to the apparent brightnesses of the QSOs, we are able to constrain the presence/absence of Mg II absorbers with rest-frame absorption equivalent width $W_r(2796) \gtrsim 0.3 \text{ \AA}$ for $\gtrsim 35\%$ of the total LRG sample. The unprecedentedly large LRG-QSO pair sample allows us to accurately determine the mean incidence of extended Mg II gas around these massive galaxies as a whole. In addition, it enables a detailed study of how the incidence and covering fraction of chemically-enriched cool gas depend on the projected distance from central LRGs and on additional galaxy properties, such as mass, emission-line properties, and geometric alignments. These observations provide important insights into the origin of the observed chemically-enriched cool gas in LRG halos.

The paper is organized as follows. In Section 2, we describe the procedures to establish the close LRG-QSO pair sample, summarize the general properties of the LRGs, and describe the absorption-line measurements. In Section 3, we inspect the photometric and spectral properties of the LRGs and examine whether/how the observed Mg II absorption strength and covering fraction in LRG halos are correlated with galaxy properties. Finally in Section 4, we consider different scenarios that can explain the presence of chemically-enriched cool gas in the massive halos where these evolved galaxies reside. We adopt a standard Λ cosmology, $\Omega_M = 0.3$ and $\Omega_\Lambda = 0.7$ with a Hubble constant $H_0 = 70 \text{ km s}^{-1} \text{ Mpc}^{-1}$.

2 DATA

We utilize existing spectroscopic data in the public SDSS archive to characterize the CGM of massive galaxies. Here we describe the procedures that we followed for establishing the projected LRG and QSO pair catalog and summarize the general properties of the LRGs in the pair sample. In addition, we describe the absorption-line measurements that led to important constraints for the CGM around LRGs.

2.1 The LRG-QSO Pair Catalog

We first considered the galaxies and quasars from the Data Release (DR12, Alam et al. 2015) of SDSS, particularly those in the Baryon Oscillation Spectroscopic Survey (BOSS, Dawson et al. 2013). In total, imaging and spectroscopic data were obtained in BOSS for ~ 1.5 million luminous galaxies at mean redshift $\langle z \rangle \approx 0.6$. The quasar sample includes about 150k quasars from both SDSS-II and BOSS at $z < 3.5$. The new BOSS multi-object spectrograph

¹ We note a critical distinction between Mg II -selected galaxy surveys and galaxy-centric absorber searches. The former, Mg II -selected galaxy surveys, address questions regarding the origin of detected Mg II absorbers (e.g., Steidel et al. 1994, 1997), while the latter, galaxy-centric absorber searches, address the incidence and covering fraction of Mg II absorbing gas around known galaxies. Including Mg II -absorbing galaxies uncovered from absorber-selected studies would naturally introduce significant scatter and bias the observed gas covering fraction to higher values.

Table 1. Definitions of Various Spectral Indices

Index	Line passband (Å)	Blue continuum (Å)	Red continuum (Å)	Reference
[O II]	3713.0 – 3741.0	3653.0 – 3713.0	3741.0 – 3801.0	Balogh et al. (1999)
D4000	...	3850.0 – 3950.0	4000.0 – 4100.0	Balogh et al. (1999)
H δ_A	4083.5 – 4122.3	4041.6 – 4079.8	4128.5 – 4161.0	Worthey & Ottaviani (1997)
[O III]	4998.2 – 5018.2	4978.2 – 4998.2	5018.2 – 5038.2	Yan et al. (2006)
H α	6554.6 – 6574.6	6483.0 – 6513.0	6623.0 – 6653.0	Yan et al. (2006)
[N II]	6575.3 – 6595.3	6483.0 – 6513.0	6623.0 – 6653.0	Yan et al. (2006)

(Smee et al. 2013) covers a wavelength range from 3600 Å to 10400 Å, and enables observations of Mg II absorbers at redshifts from as low as $z \approx 0.28$ to $z \approx 2.7$. We cross-matched spectroscopically identified galaxies with background quasars to find projected pairs separated by $d < 500$ kpc in projected distance. The background quasars and foreground galaxies are drawn from the BOSS automated spectral classification and redshift measurement pipeline (Bolton et al. 2012). The maximum projected distance of $d = 500$ kpc is chosen based on the expected size of a typical LRG host dark matter halo. We excluded galaxies that occur within a line-of-sight velocity separation of $< 10,000$ km s $^{-1}$ from the background QSO in order to exclude correlated QSO–galaxy pairs and to avoid confusions between absorption features imprinted by the CGM of LRGs and by QSO outflows. The process yielded a total of 45757 galaxies at $d < 500$ kpc from the sightline of a background QSO in the SDSS sample. Redshifts of the galaxies range from $z = 0.30$ to $z = 1.42$. Note that due to BOSS galaxy target selection, this galaxy sample consists of $\approx 83\%$ LRGs and $\approx 17\%$ luminous star-forming galaxies.

The spectroscopic targets of two primary BOSS galaxy samples, LOWZ ($z \lesssim 0.4$) and CMASS ($0.4 \lesssim z \lesssim 0.7$), were selected using two sets of color-magnitude cuts similar to the LRG target selection for SDSS-I/II (Eisenstein et al. 2001). A crucial difference is that the CMASS sample extends the SDSS-I/II LRG selection to include blue objects. As a result, while the majority of targeted galaxies are LRGs, there is a non-negligible number of massive star-forming galaxies that could potentially bias our results. To identify LRGs from the initial BOSS galaxy sample, we further applied a color selection criterion based on the intrinsic, rest-frame $u - g$ color. Using the Sbc galaxy template of Coleman et al. (1980), we defined elliptical galaxies as those with rest-frame $u - g$ color redder than the Sbc template, and star-forming galaxies as those with bluer $u - g$ colors. Specifically,

$$\begin{aligned} u - g &> 1.18 && \text{for elliptical/S0} \\ u - g &\leq 1.18 && \text{for disk/irregular/star-forming galaxies} \end{aligned} \quad (1)$$

The rest-frame $u - g$ color of each galaxy was computed based on its spectroscopic redshift from BOSS and interpolating between u -, g -, r -, i -, and z -band composite model magnitudes from the SDSS archive. In addition to the rest-frame $u - g$ color selection, we also restricted the sample selection to galaxies that do not exhibit strong interstellar medium emission lines due to [O II] $\lambda 3727$, [O III] $\lambda 5007$, or H α $\lambda 6564$ at more than $5\text{-}\sigma$ level of significance. Some of these galaxies displayed both dominant absorption features due to an evolved stellar population and strong emission lines from H II regions. The choice of a $5\text{-}\sigma$ threshold is to

ensure that we do not exclude more than 1% of evolved galaxy populations. Details of measuring equivalent widths of galaxy emission lines are presented in Section 3.1 and definitions of various spectral indices are summarized in Table 1. Applying these additional cuts yielded a total of 38116 LRGs and $\lesssim 0.2\%$ contamination by galaxies with younger stellar populations based on visual inspections. As described in the next section (§ 2.2), 495 of these LRGs occur at a redshift where the spectrum of the background QSO does not provide useful constraints for the halo gas content. Excluding these LRG-QSO pairs led to a final sample of 37621 LRGs for the subsequent CGM studies.

To characterize the general properties of these LRGs, we computed the rest-frame absolute r -band magnitude M_r and stellar mass M_* based on the observed SDSS g -, r -, i -, and z -band magnitudes, using the K -correct code (Blanton & Roweis 2007). We excluded the u -band from the photometric analysis, because $\approx 99\%$ of the LRGs are not detected at $\geq 5\sigma$ level of significance in the u -band. Distributions in redshift, M_r , and M_* for the full sample are presented in Figure 1 in filled histograms. The redshift distribution of our LRGs (left panel of Figure 1) clearly shows a double-peak feature, with the majority selected from the CMASS sample at $z = 0.4 - 0.7$ and some fraction from the SDSS LOWZ sample at $z \lesssim 0.4$. We note, however, that a substantial fraction of LRGs from the LOWZ program do not have sensitive constraints for their associated Mg II absorption features, because at this redshift range the Mg II doublet transitions occur at $\lambda < 4000$ Å, where the throughput of the spectrograph declines rapidly (Smee et al. 2013). Stellar masses of the full LRG sample span a range from $\log M_*/M_\odot < 11$ to $\log M_*/M_\odot \approx 12$ (right panel of Figure 1) with a mean of $\langle \log M_*/M_\odot \rangle = 11.4$ and a dispersion of 0.2 dex.

While LRGs exhibit spectral features that are typical of an old and passively evolved stellar population, roughly 10% of the LRG population also exhibit emission lines from recent star formation or AGN activity (e.g. Roseboom et al. 2006). To isolate quiescent galaxies with little/no on-going star formation, we further divided the final LRG sample into two subsamples based on the significance of the observed [O II] emission. The procedure yielded 4994 LRGs with [O II] detected at greater than $2\text{-}\sigma$ level of significance, and 32627 passive LRGs without detected [O II].

In subsequent discussions, we focus our analysis on a subsample of LRGs for which sensitive constraints for their halo gas content can be placed using the spectrum of a background QSO (more details are described in Section § 2.2). Considering only LRGs with sufficiently high S/N background QSO spectra for detecting Mg II absorbers as weak as $W_0 = 0.3$ Å led to a total sample of 13330 LRGs

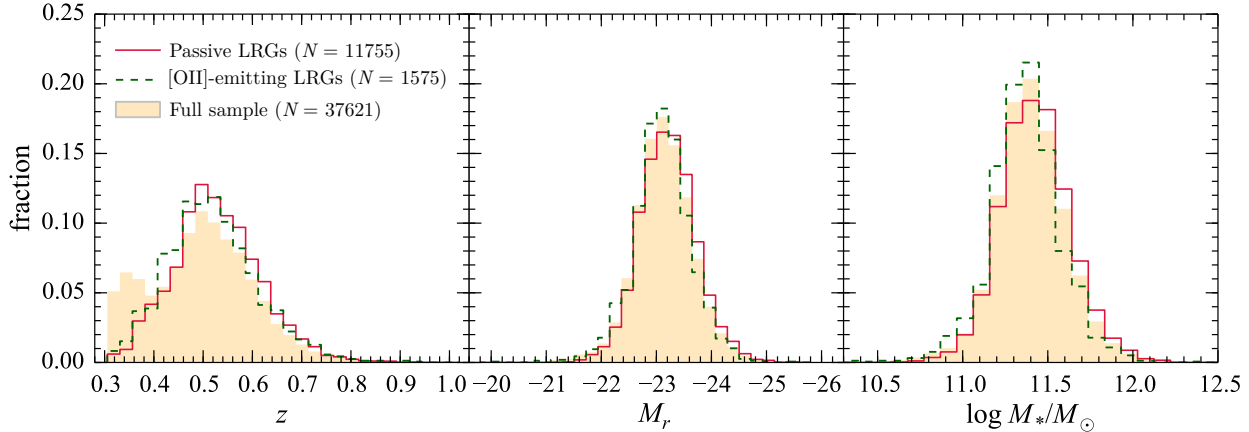


Figure 1. Distributions in redshift z , r -band absolute magnitude M_r , and stellar mass M_* of LRGs in our study. The full sample consists of 37621 LRGs from a combination of SDSS LOWZ sample that dominates the LRG population at $z \lesssim 0.4$ and the CMASS sample that dominates at $z = 0.4 - 0.7$ (left panel). Considering only LRGs with sufficiently high S/N background QSO spectra for detecting Mg II absorbers as weak as $W_0 = 0.3 \text{ \AA}$ yields a total sample of 13330 LRGs, 1575 of which are [O II]-emitting (open, dashed histograms) and 11755 are passive LRGs with no trace of [O II] emission at more than a $2\text{-}\sigma$ level of significance (open, red histograms). The redshift distributions of these LRGs show that the $W_0 = 0.3 \text{ \AA}$ cut removes a significant fraction of LRGs from the LOWZ sample, due to the rapidly declining throughput at $\lambda \lesssim 4000 \text{ \AA}$ of the SDSS spectrograph (Smee et al. 2013) that prohibited us from detecting relatively weak Mg II absorption features at $z \lesssim 0.4$. All three LRG samples share similar distributions in M_r (middle panel) and M_* (right panel).

(Table 2). Figure 1 demonstrates that for LRGs with sensitive absorption-line constraints, both passive (open, red histograms) and [O II]-emitting (open, dashed histograms) LRGs exhibit similar distributions in redshift, M_r , and M_* . Specifically, [O II]-emitting LRGs span a range in redshift from $z = 0.31$ to $z = 0.94$ with a median of $\langle z \rangle_{\text{med}} = 0.51$, while passive LRGs cover a redshift range from $z = 0.31$ to $z = 0.99$ with $\langle z \rangle_{\text{med}} = 0.52$. In terms of stellar mass, [O II]-emitting LRGs are well described by a Gaussian distribution with a mean of $\langle \log(M_*/M_\odot) \rangle = 11.37$ and a dispersion of 0.18 dex while passive LRGs without detected [O II] are well described by a Gaussian distribution of $\langle \log(M_*/M_\odot) \rangle = 11.42$ and a dispersion of 0.2 dex (Table 2). The difference in the mean stellar masses is negligible, given the ≈ 0.2 dex scatter introduced in estimating photometric stellar masses (Blanton & Roweis 2007).

Finally, we note that the previous $5\text{-}\sigma$ equivalent width cut had excluded $\sim 1\%$ of strong [O II]-emitting LRGs with underlying old stellar populations. Including these strong [O II]-emitting LRGs will not significantly alter the statistical properties of [O II]-emitting LRGs in our sample, but will likely increase the differences found in the CGM between [O II]-emitting and non-[O II]-emitting LRGs. We defer the analysis of those strong [O II]-emitting LRGs to a future paper.

2.2 Extended Mg II Halos around LRGs

To constrain the halo gas content of LRGs, we took each projected LRG–QSO pair from § 2.1 and manually searched for the corresponding Mg II absorption features at the redshift of the LRG in the spectrum of the background QSO. Our search window covers a radial velocity interval of $\Delta v = \pm 1000 \text{ km s}^{-1}$, centered at the systemic redshift of the LRG. This large search window was chosen to include the vast majority of Mg II absorption systems originating in LRG halos. It is based on the expected velocity dispersion of $\sigma \sim 350$

km s^{-1} for virialized gas in halos of $\sim 10^{13} M_\odot$. In addition, as described in § 3.2 below, the detected Mg II absorbers exhibit a simple Gaussian distribution in velocity offset from the systemic redshifts of the LRGs, which is characterized by a velocity dispersion of $\sigma_v \approx 165 \text{ km s}^{-1}$ (see Figure 3 below). We are therefore confident that the adopted search window was sufficiently large to find associated absorbers.

When a Mg II absorber was found in the QSO spectrum, we measured the rest-frame absorption equivalent width of the 2796 Å member, $W_r(2796)$, and determined the absorber redshift based on the best-fit line centroid of a Gaussian profile. For 20 LRGs, multiple Mg II absorbers were found within the search window. We adopt the velocity centroid of the strongest component as the systemic velocity of the absorbing gas. When no Mg II features were detected, we record a $2\text{-}\sigma$ upper limit of the underlying absorber strength over a wavelength window defined by the width of a spectral resolution element of SDSS spectra ($\text{FWHM} = 150 \text{ km s}^{-1}$), based on the associated $1\text{-}\sigma$ error spectrum.

In the full LRG sample, two groups of LRGs were found to have corresponding Mg II absorbers within $\Delta v < 1000 \text{ km s}^{-1}$. For these two cases, we assigned absorbers to the LRGs at the smallest projected distance and excluded the remaining LRGs from the sample. The procedure identified 710 Mg II absorbers and 36911 upper limits in the vicinities of 37621 LRGs. We were unable to obtain significant constraints for Mg II absorbers around 478 LRGs, where the accompanying QSO spectra have extraction defects, broad absorption line complexes, or are contaminated by other absorption transitions (such as C IV $\lambda\lambda 1548, 1550$) from a different redshift. For 17 LRGs, the corresponding Mg II absorption was expected to fall close to a prominent QSO emission line. Because of significant uncertainties in the continuum near the peak of a QSO emission line, these LRGs are also excluded from the analysis.

The constraints we were able to place for the presence or absence of extended Mg II absorbing gas around the LRGs

Table 2. Summary of the LRG Samples

W_0 (Å)	LRG Type	$N(\text{total})$	$N(\text{upper limit})$	$N(\text{detection})$	$\langle \log M_*/M_\odot \rangle$	$\sigma(\langle \log M_*/M_\odot \rangle)$
Any	Full	37621	36911	710	11.40	0.19
0.3	[O II]-emitting	1575	1499	76	11.37	0.18
0.3	Passive	11755	11215	540	11.42	0.20
0.3	All	13330	12714	616	11.42	0.20

were also non-uniform. Because of varying qualities (in terms of S/N) of the absorption spectra at different wavelengths and between different QSOs, there exists a substantial scatter in the upper limits we were able to place for those 36911 LRGs. For a large fraction of the LRGs ($\approx 2/3$ of the sample), the apparent, low S/N spectra of the QSOs prohibited us from placing sensitive constraints for the underlying Mg II absorbers.

To facilitate a uniform analysis, we focused our subsequent studies on a homogeneous sample of LRGs with sufficiently high S/N background QSO spectra that allow a minimum detection threshold in rest-frame absorption equivalent width of $W_0 = 0.3$ Å for the Mg II absorption features. A summary of the LRG samples and the Mg II survey result is shown in Table 2. Under the $W_0 = 0.3$ Å minimum quality cut, we have a sample of 11755 passive LRGs without [O II] detected at a more than $2\text{-}\sigma$ level and 1575 [O II]-emitting LRGs. The fraction of [O II]-emitting LRGs ($\approx 13\%$) is consistent with what was found in the 2dF–SDSS LRG and QSO Survey (Roseboom et al. 2006).

To compare the general properties of the [O II]-emitting and passive LRG samples, we include their distributions in redshift, M_r and M_* in Figure 1 and Table 2. The passive LRGs with sensitive Mg II absorption constraints are shown in open, red histograms, and the [O II]-emitting LRGs are shown in dashed, green histograms. The comparisons confirm that with the additional $W_0 = 0.3$ Å selection criterion, the underlying redshift and M_* distributions of the resulting [O II]-emitting and passive LRG subsamples remain the same.

3 ANALYSIS

The procedures described in Section 2 established a sample of 13330 LRGs with sensitive background QSO spectra available for constraining the presence/absence of Mg II absorbers of $W_r(2796) \geq 0.3$ Å. Of these, 1575 show [O II] emission in the LRG spectra and 11755 LRGs appear to contain a passive and old stellar population with no [O II]-emission detected at greater than a $2\text{-}\sigma$ level. As summarized in Table 2, the passive and [O II]-emitting LRGs share a very similar distribution in stellar mass with a mean of $\langle \log M_*/M_\odot \rangle = 11.4$ and a dispersion of 0.2 dex (see also the right panel of Figure 1). In addition, our search of Mg II absorption features in the vicinities of these LRGs yielded 76 detections around [O II]-emitting LRGs (a rate of incidence $\approx 4.8\%$) and 540 detections around passive LRGs ($\approx 4.6\%$).

In this section, we first inspect the general properties of passive and [O II]-emitting LRG samples, focusing primarily on their respective stellar populations and star formation histories. Then we examine Mg II absorption properties

in LRG halos and investigate possible correlations between LRG properties and the observed Mg II absorption properties in LRG halos.

3.1 Mean Stellar Populations of the LRGs

While LRGs are generally understood as high-redshift counterparts of nearby massive elliptical galaxies that are made of predominantly old stellar populations with little/no star formation, the visual inspection described in § 2.1 has confirmed previous findings that roughly 10% of these LRGs exhibit [O II] emission features that suggest a modest amount of star formation among otherwise evolved stellar populations (e.g. Roseboom et al. 2006). Because a primary goal of targeting gaseous halos around LRGs is to investigate whether and how chemically-enriched absorbing gas can arise at large distances from evolved galaxies in the absence of active on-going star formation, it is necessary to first characterize the mean star formation history and mean stellar population of [O II]-emitting and passive LRG samples before discussing the properties of their halo gas content.

To examine the stellar population, we form a stacked spectrum of each of the LRG subsamples and measure its spectral properties. To generate a stacked spectrum, we first mask out strong sky emission lines. We then shift the observed spectrum to the rest frame of the galaxy and adopt a constant pixel resolution of $\Delta \lambda = 2$ Å, corresponding to roughly $\Delta v = 150$ km s $^{-1}$ at 4000 Å, and 75 km s $^{-1}$ at 8000 Å. Individual LRG spectra were normalized using the mean flux over $\lambda = 4100 - 4300$ Å, and median combined to form the final stacked spectrum.

For each stacked spectrum, we measure the D4000 index and the equivalent widths of [O II], H δ_A , H α , and [N II] lines. For each emission line, the continuum is determined by measuring the mean flux level in two sidebands and interpolating across the central passband. Then we sum over the continuum-normalized flux in the central passband to obtain the equivalent width of the line. For [O II] and H δ , we use the standard definitions from Balogh et al. (1999) and Worthey & Ottaviani (1997), respectively. For H α and [N II], we adopt the window definitions from Yan et al. (2006). We define the D4000 index using the narrow definition introduced by Balogh et al. (1999), namely the ratio of the fluxes in two 100-Å windows centered at 4050 and 3900 Å. The definitions of the passbands and sidebands are summarized in Table 1.

To estimate uncertainties in the measured line indices, we perform a bootstrap analysis and repeat the stacking procedure 1000 times. We record the $1\text{-}\sigma$ dispersions in the measured spectral indices as the measurement uncertainties. The results are summarized in Table 3. We have also

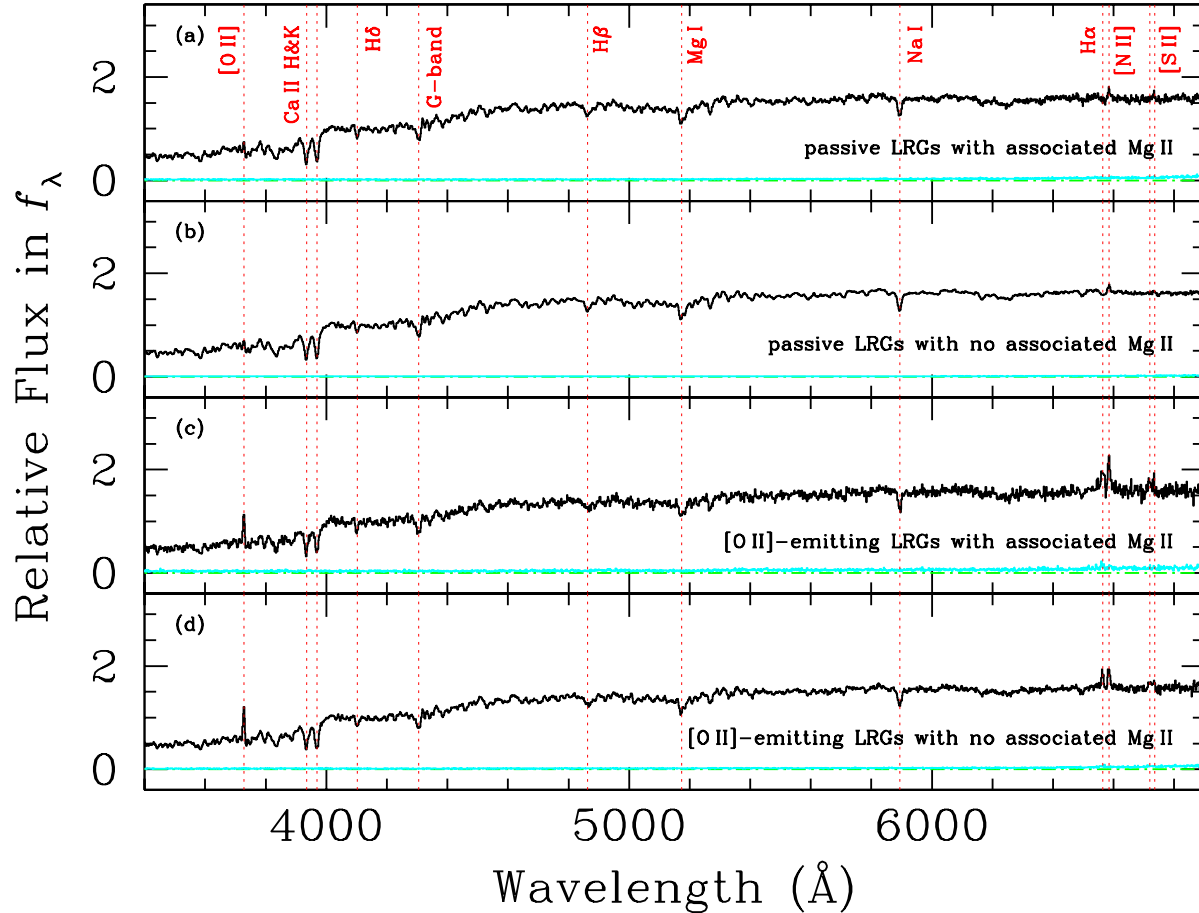


Figure 2. Stacked rest-frame spectra of LRGs at $d < 200$ kpc from a background QSO sightline with sufficiently high S/N absorption spectra available for detecting a Mg II absorber of $W_r(2796) > 0.3$ Å. The corresponding $1-\sigma$ dispersion in each stack is shown in cyan at the bottom of each panel. Panel (a) shows the median stack of 204 passive LRGs with associated Mg II absorbers, and panel (b) displays the median stack of 1567 passive LRGs without associated Mg II absorbers. The stacked spectra are characterized by prominent absorption features due to Ca II H & K, G-band, Mg I and Na I that indicate a predominantly old stellar population, as well as a relatively weak Balmer absorption series. Neither [O II] nor H α emission line is detected in the stacks but we note the presence of [N II] λ 6585 emission. Panels (c) and (d) display the stacked spectra of [O II]-emitting LRGs with and without associated Mg II absorbers, respectively. A total of 41 LRG spectra are included in the stack presented in panel (c) and 240 LRGs in panel (d). Similar to passive LRGs, the stacked spectra of [O II]-emitting LRGs display prominent absorption features that indicate the presence of evolved stellar populations, but at the same time modest emission features due to H α , [N II], and [S II] are also detected. The observed relatively weak H α emission together with a prominent [N II] λ 6585 emission feature suggests a subdominant presence of LINERs.

Table 3. Summary of LRG properties from stacked spectra

Spectral Type (1)	Mg II Absorption (2)	D4000 (3)	EW([O II]) (Å) (4)	EW(H δ_A) (Å) (5)	EW(H α) ^a (Å) (6)	EW([N II]) (Å) (7)	SFR _{Hα} ^b (M $_{\odot}$ /yr) (8)
Passive LRGs	detection	1.63 ± 0.01	0.61 ± 0.28	1.44 ± 0.13	-1.46 ± 0.26	-1.18 ± 0.19	0.48 ± 0.09
Passive LRGs	non-detection	1.64 ± 0.01	0.78 ± 0.10	1.05 ± 0.04	-1.03 ± 0.08	-0.80 ± 0.06	0.34 ± 0.03
[O II]-emitting LRGs	detection	1.53 ± 0.03	-5.45 ± 0.53	2.02 ± 0.39	-4.24 ± 0.94	-4.19 ± 0.48	1.40 ± 0.31
[O II]-emitting LRGs	non-detection	1.52 ± 0.01	-4.98 ± 0.24	1.77 ± 0.15	-3.28 ± 0.33	-2.70 ± 0.19	1.08 ± 0.11

^aCorrected for stellar absorption based on a fit to the higher-order Balmer absorption series.

^bBased on the assumption that the observed H α emission traces young stars and applying the scaling relation of Kennicutt & Evans (2012). But because the observed emission-line ratios resemble LINER-like galaxies (e.g., Yan et al. 2006), the inferred SFR represent only an upper limit.

experimented with forming a mean (rather than median) stack and found that the measurements remain consistent within uncertainties. Note that throughout this paper we define a negative equivalent width as emission and a positive value as absorption.

The resulting median stacks of LRG spectra are pre-

sented in Figure 2, including passive LRGs with associated Mg II absorbers in panel (a), passive LRGs without associated Mg II absorbers in panel (b), [O II]-emitting LRGs with detected Mg II absorbing gas in panel (c), and [O II]-emitting LRGs without associated Mg II absorbers in panel (d). The stacked spectra presented in Figure 2 include only LRGs

that occur at $d < 200$ kpc from a background QSO sightline with sufficiently high S/N absorption spectra available for detecting a Mg II absorber of $W_r(2796) > 0.3 \text{ \AA}$. This is motivated by the apparent difference in the observed covering fraction of Mg II absorbers at $d < 200$ kpc around different LRG samples, as shown in the following section (§ 3.2). The goal is to examine whether the observed difference in extended Mg II absorbing gas is related to the stellar population in the galaxies.

Figure 2 shows that all the LRG samples exhibit prominent absorption features due to Ca II H & K, G band, Mg I and Na I, indicating that the spectra are dominated by old stellar populations. We make use of the $H\delta_A$ and D4000 spectral indicators as diagnostics of recent star formation histories. The D4000 index is known to be sensitive to recent star formation, with lower values indicating an increasing presence of a young stellar population. The $H\delta$ absorption line, on the other hand, occurs in galaxies that have experienced a burst of star formation $\sim 0.1 - 1$ Gyr ago. The absorption strength is expected to peak at ~ 1 Gyr when hot O and B stars have left the main sequence, and decline with increasing age afterward. The [O II]-emitting LRGs have $D4000 \approx 1.5$ and $H\delta$ equivalent width of $EW(H\delta_A) \approx 2$, whereas passive LRGs have $D4000 \approx 1.6$ and $EW(H\delta_A) \approx 1.2$. No significant difference is found for the D4000 index and only marginal difference is seen in $H\delta$ between Mg II -absorbing and non-absorbing passive LRGs.

Following the diagnostics described in Kauffmann et al. (2003), we estimate a mean stellar age of $\gtrsim 1$ Gyr based on the mean spectral indices observed in the stacked LRG spectra. The estimated mean stellar age is consistent with the conclusions of Gauthier & Chen (2011) for 37 individual LRGs based on a stellar population synthesis analysis. If the [O II]-emitting and passive LRG samples share a similar metallicity, then the smaller mean D4000 indices and higher $EW(H\delta)$ in [O II]-emitting LRGs suggest an on average younger stellar population in these galaxies than in passive LRGs.

We also investigate the emission line properties of different LRG samples. For passive LRGs, we do not uncover [O II] emission even in the high S/N stacked spectra. For [O II]-emitting LRGs, we uncover relatively weak $H\alpha$ emission in the stacked spectra. Both passive and [O II]-emitting LRGs exhibit a modest [N II] $\lambda 6585$ emission feature. After correcting for stellar absorption using the observed $H\beta$, $H\gamma$, and $H\delta$ absorption features, we recover the underlying $H\alpha$ emission flux for all LRG subsamples. The stellar absorption-corrected $H\alpha$ emission equivalent width for each subsample is presented in column (6) of Table 3. Assuming that the observed $H\alpha$ emission traces on-going star-formation in the LRGs and applying the scaling relation from Kennicutt & Evans (2012), we infer an unobscured star formation rate (SFR) based on the observed $EW(H\alpha)$ and mean M_r . The estimated mean $SFR_{H\alpha}$ of each LRG sample is presented in Table 3. We find that [O II]-emitting LRGs have a mean SFR as high as $SFR_{H\alpha} \approx 1 - 1.5 M_\odot \text{ yr}^{-1}$ and passive LRGs have a mean SFR as high as $SFR_{H\alpha} \approx 0.3 - 0.4 M_\odot \text{ yr}^{-1}$.

However, many local elliptical galaxies and passive red galaxies at higher redshifts display emission features that resemble the low-ionization nuclear emission-line regions (LINERs; e.g., Sarzi et al. 2006; Yan et al. 2006). Searches for radio emission based on stacks of FIRST images of the

LRGs have also continued to uncover faint radio fluxes in these galaxies (e.g., Hodge et al. 2008, 2009). The observed high [N II] / $H\alpha$ ratio, together with a low [O III] / [O II] ratio, in our stacked spectra of [O II]-emitting galaxies (bottom two panels of Figure 2) indeed confirms previous findings that these LRGs are LINER-like galaxies (e.g. Johnston et al. 2008; Hodge et al. 2008). Therefore, the observed [O II] and $H\alpha$ emission features are most likely due to underlying active galactic nuclei (AGN) or LINERs, and the SFR estimated based on the observed $H\alpha$ emission flux only represents an upper limit.

3.2 Properties of Mg II Absorbing Gas in LRG Halos

To examine Mg II absorption properties in LRG halos, we first compare the observed Mg II absorption strength with the projected distance between the absorbing gas and the galaxy. Figure 3 shows the distribution of $W_r(2796)$ versus projected distance d to the LRGs. We present the observations for passive and [O II]-emitting LRGs in separate panels for a direct comparison of the CGM properties between galaxies with different star formation properties (see the discussion in the previous section, § 3.2). We focus on the subsample of LRGs with sufficiently high S/N background QSO spectra for detecting Mg II absorbers as weak as $W_0 = 0.3 \text{ \AA}$. A significant fraction of the original SDSS LRG sample have poorer-quality QSO spectra that result in upper limits exceeding 0.3 \AA . As a result, these LRG-QSO pairs offer little/no constraints for the underlying absorber strengths in LRG halos and are therefore excluded from the panels for clarity.

Both panels in Figure 3 show that the LRGs with associated Mg II absorbers occupy a similar $W_r(2796)$ versus d space. Although many LRGs show no detectable Mg II absorbers of $W_r(2796) \geq 0.3 \text{ \AA}$, a non-negligible fraction of LRGs show strong associated Mg II absorbers of $W_r(2796) \sim 1 \text{ \AA}$ out to $d = 500$ kpc, the virial radii of LRG host dark matter halos. While strong Mg II absorbers are also found at large distances from QSOs (e.g., Johnson et al. 2015), such flat $W_r(2796)$ versus d trend is in stark contrast to known halo gas properties around L_* galaxies. These strong absorbers are only found around L_* galaxies at $d \lesssim 60$ kpc, beyond which the observed Mg II absorbing strength rapidly declines (e.g., Chen & Tinker 2008; Chen et al. 2010a).

As described in § 2.1, the LRGs span a range in stellar mass from $\log M_*/M_\odot < 11$ to $\log M_*/M_\odot \approx 12$ (right panel of Figure 1) with a mean of $\langle \log M_*/M_\odot \rangle = 11.4$ and a dispersion of 0.2 dex. It is possible that the relatively broad range in stellar mass contributes to the observed flat trend in $W_r(2796)$ versus d . We perform two tests to examine whether this is a factor. First, we compare the stellar mass distributions of Mg II -absorbing and non-absorbing LRGs. We find that both Mg II -absorbing and non-absorbing LRGs are well characterized by a Gaussian distribution function with a mean of $\langle \log M_*/M_\odot \rangle = 11.4$ and a dispersion of 0.2 dex. We therefore do not find a preference of Mg II absorbers around low- or high-mass LRGs. Next, we include the stellar mass scaling relation found for L_* galaxies by Chen et al. (2010b) and examine whether the observed scatter in $W_r(2796)$ versus d is reduced. The result shows that including stellar mass scaling does not improve/reduce

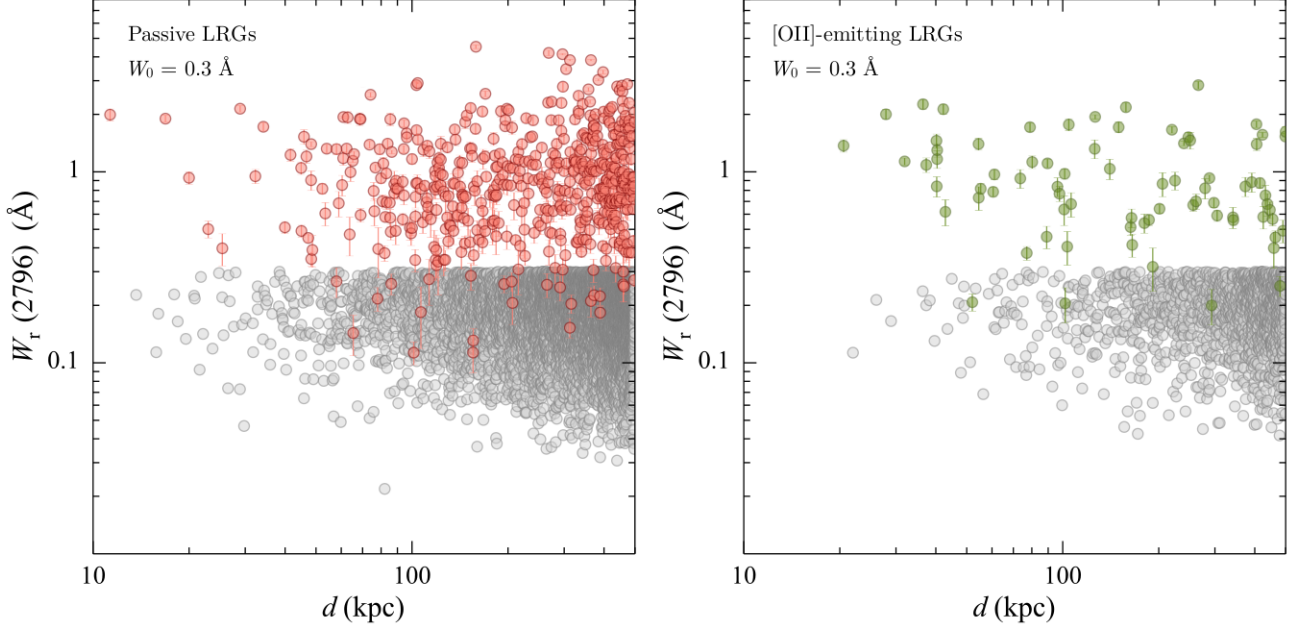


Figure 3. Rest-frame absorption equivalent width $W_r(2796)$ versus projected distance d for LRGs with sufficiently high S/N background QSO spectra for detecting Mg II absorbers as weak as $W_0 = 0.3 \text{ \AA}$. Absorption observations for passive LRGs are shown in the *left* panel. Observations of [O II]-emitting LRGs are shown in the *right* panel. LRGs with detected Mg II absorbers are shown in filled circles with errorbars representing measurement uncertainties. For non-detections, we use light grey circles to indicate the $2\text{-}\sigma$ upper limits. Note that a significant fraction of the original SDSS LRG sample have poor-quality QSO spectra that result in upper limits exceeding 0.3 \AA . These LRG–QSO pairs offer little/no constraints for the underlying absorber strengths in LRG halos and are therefore excluded from the plots for clarity.

the scatter in the observed $W_r(2796)$ versus d relation. Both tests confirm that extended Mg II -absorbing gas does not depend strongly on the mass of the LRGs.

At the same time, we also examine the velocity dispersion of the detected absorbing gas around LRGs. The left panel of Figure 4 shows the relative line-of-sight velocity distributions of Mg II absorbers with respect to the systemic redshifts of LRGs at $d < 500 \text{ kpc}$. Following the presentation in Figure 3, we present the velocity distribution separately for passive and [O II]-emitting LRGs. The velocity distribution of Mg II absorbing gas around [O II]-emitting LRGs can be characterized by a single Gaussian distribution of mean velocity difference $\langle v_{\text{Mg II-Galaxy}} \rangle = -5 \text{ km s}^{-1}$ and dispersion $\sigma_v = 167 \text{ km s}^{-1}$ (green dashed curve). However, the velocity distribution of Mg II absorbing gas around passive LRGs without detectable [O II] emission features appears to have extended, high-velocity wings and is best represented by a double Gaussian profile with a narrow component centered at $\langle v_{\text{Mg II-Galaxy}} \rangle = -3 \text{ km s}^{-1}$ and $\sigma_v = 163 \text{ km s}^{-1}$ and a broad component centered at $\langle v_{\text{Mg II-Galaxy}} \rangle = -17 \text{ km s}^{-1}$ and $\sigma_v = 415 \text{ km s}^{-1}$ (red solid curve). We find that 62 Mg II absorbers occur at $|v_{\text{Mg II-Galaxy}}| > 500 \text{ km s}^{-1}$ from passive LRGs, which constitute $(12 \pm 1)\%$ of the total Mg II -absorbing passive LRG sample.

To evaluate whether the observed velocity dispersion vary with projected distance, we consider only LRGs with a Mg II absorber found at $d < 200 \text{ kpc}$ from LRGs. Of the 540 passive LRGs–Mg II absorber pairs in Table 2, 208 are separated by $d < 200 \text{ kpc}$. Of the 76 [O II]-emitting LRGs–Mg II absorber pairs, 42 are separated by $d < 200 \text{ kpc}$. The right panel of Figure 4 shows the line-of-sight veloc-

ity distribution of Mg II absorbers relative to the LRGs at $d < 200 \text{ kpc}$. We find similar characteristics in the velocity distribution of Mg II absorbing gas at smaller projected distances from LRGs. For [O II]-emitting LRGs, a single Gaussian function is sufficient to describe the line-of-sight gas motion with a mean of $\langle v_{\text{Mg II-Galaxy}} \rangle = +6 \text{ km s}^{-1}$ and dispersion $\sigma_v = 150 \text{ km s}^{-1}$ (green dashed curve in Figure 4). For passive LRGs, high-velocity Mg II absorbers are also seen but at a reduced fraction. We find that 13 out of 208 Mg II absorbers at $d < 200 \text{ kpc}$ occur at $|v_{\text{Mg II-Galaxy}}| > 500 \text{ km s}^{-1}$, which constitute $(6 \pm 2)\%$ of [O II]-emitting LRGs with associated Mg II. The best-fit double Gaussian profile is characterized by a narrow component centered at $\langle v_{\text{Mg II-Galaxy}} \rangle = -15 \text{ km s}^{-1}$ and $\sigma_v = 170 \text{ km s}^{-1}$ and a broad component centered at $\langle v_{\text{Mg II-Galaxy}} \rangle = +6 \text{ km s}^{-1}$ and $\sigma_v = 453 \text{ km s}^{-1}$ (red solid curve in Figure 4). The increasing fraction of high-velocity ($|v_{\text{Mg II-Galaxy}}| > 500 \text{ km s}^{-1}$) Mg II absorbers from $d < 200$ to larger distances may be understood by an increasing fraction of contaminating random background or correlated absorbers outside the LRG halos as the projected distance increases.

Figure 4 shows that Mg II absorbing gas detected around passive and [O II]-emitting LRGs (particularly the absorbers found at $d < 200 \text{ kpc}$) shares a similar line-of-sight velocity dispersion of $\sigma_v \approx 165 \text{ km s}^{-1}$. The velocity field of chemically-enriched gas in massive LRG halos does not exhibit traceable dependence on the presence/absence of on-going star formation in the galaxies. Furthermore, we note that the mean halo mass of LRGs is $\langle M_h(\text{LRG}) \rangle \approx 10^{13.4} M_\odot$ (e.g. Mandelbaum et al. 2008; Gauthier et al. 2009). The expected line-of-sight velocity dis-

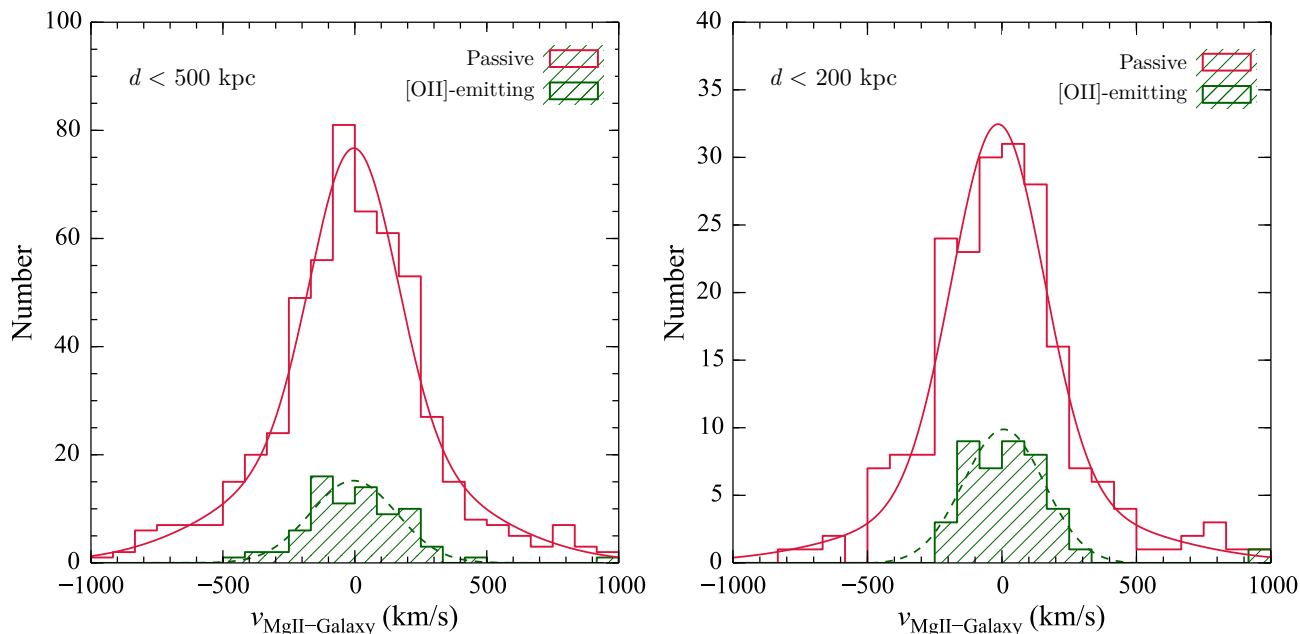


Figure 4. Relative velocity distributions of Mg II absorbers with respect to the systemic redshifts of the LRGs. Passive LRGs are shown in the red open histogram, while [O II]-emitting LRGs are shown in the green hatched histogram. The left panel includes all Mg II absorbers at $d < 500$ kpc, and the right panel includes only those at $d < 200$ kpc. Mg II absorbing gas around [O II]-emitting LRGs at $d < 500$ (200) kpc is well characterized by a single Gaussian distribution centered at $\langle v_{\text{Mg II-Galaxy}} \rangle = -5$ (+6) km s^{-1} with a dispersion of $\sigma_v = 167$ (150) km s^{-1} (green, dashed curve). Mg II absorbing gas around passive LRGs exhibits a similar distribution but with a substantial fraction, $(12 \pm 1)\%$ at $d < 500$ kpc and $(6 \pm 2)\%$ at $d < 200$ kpc, extended beyond $|v_{\text{Mg II-Galaxy}}| = 500$ km s^{-1} from the systemic redshifts of the galaxies. Applying a double Gaussian profile to characterize the velocity distribution of Mg II gas around passive LRGs at $d < 500$ (200) kpc leads to a narrow component centered at $\langle v_{\text{Mg II-Galaxy}} \rangle = -3$ (-15) km s^{-1} and $\sigma_v = 163$ (170) km s^{-1} and a broad component centered at $\langle v_{\text{Mg II-Galaxy}} \rangle = -17$ (+6) km s^{-1} and $\sigma_v = 415$ (453) km s^{-1} (red solid curve).

person for virialized gas in halos of $10^{13.4} M_{\odot}$ is $\sigma_h \approx 265$ km s^{-1} . The observed velocity dispersion in Mg II absorbing gas is merely 60% of what is expected from virial motion, namely $\sigma_v \approx 0.6 \sigma_h$. A similar result has also been seen by Zhu et al. (2014), who reported a velocity bias of $\sigma_{\text{Mg II}} \approx 0.5 \sigma_h$. Such suppression in gas motion not only shows that the gas is gravitationally bound to the LRG halo but also that additional mechanisms are necessary to slow down the motion of these absorbing clouds.

3.3 Incidence and Covering Fraction of Mg II Absorbers in LRG halos

A key quantity to characterize LRG halos is the covering fraction, $\kappa_{\text{Mg II}}$, of chemically-enriched cool gas as revealed by the presence of Mg II absorbers. We employ a maximum likelihood analysis to compute the best-fit $\kappa_{\text{Mg II}}$ and its associated uncertainties as a function of projected distance d , following the formalism described in Chen et al. (2010a). The likelihood of observing an ensemble of galaxies with n showing associated Mg II and m displaying upper limits is

$$\mathcal{L}(\kappa_{\text{Mg II}}) = \langle \kappa \rangle_{\text{Mg II}}^n [1 - \langle \kappa \rangle_{\text{Mg II}}]^m \quad (2)$$

We divide the LRGs into subsamples of different projected distance intervals and compute best-fit $\kappa_{\text{Mg II}}$ and uncertainties for each projected distance bin. Figure 5 shows the estimated $\langle \kappa \rangle_{\text{Mg II}}$ versus d in intervals of 40 kpc. Error

bars in $\langle \kappa \rangle_{\text{Mg II}}$ represent the 68 per cent confidence interval based on the likelihood function. The number of LRGs in each projected distance interval is shown at the top of Figure 5. For accurate estimates of gas covering fraction, we consider only those LRGs with sufficiently high S/N background QSO spectra available for detecting Mg II absorbers as weak as $W_0 = 0.3$ Å. For investigating possible dependence of the incidence of chemically-enriched halo gas on star formation activities, we consider passive and [O II]-emitting LRGs separately.

We also estimate contamination due to background structures along the line of sight. Following Gauthier et al. (2010), we estimate the incidence of random background Mg II absorbers within a redshift interval of $\Delta z = 0.01$, corresponding to a velocity interval of $\Delta v = \pm 1000$ km s^{-1} , based on the mean number density of Mg II absorbers with $W_r(2796) \geq 0.3$ Å from Nestor et al. (2005). The ≈ 1 per cent contribution as shown in Figure 5 (dashed curve) suggests that random background absorbers have negligible impact on the observed covering fraction of Mg II absorbing gas at $d \lesssim 200$ kpc, but contribute a significant portion of Mg II absorbers found at larger distances.

Figure 5 displays a number of interesting features. First, the covering fraction of Mg II absorbers is significantly elevated in the inner halos with a mean covering fraction ranging from $\langle \kappa \rangle_{\text{Mg II}} \approx 15\%$ at $d \lesssim 120$ kpc for passive LRGs to as high as $\langle \kappa \rangle_{\text{Mg II}} \approx 40\%$ at $d \lesssim 40$ kpc for [O II]-emitting LRGs. This is in contrast to an overall covering

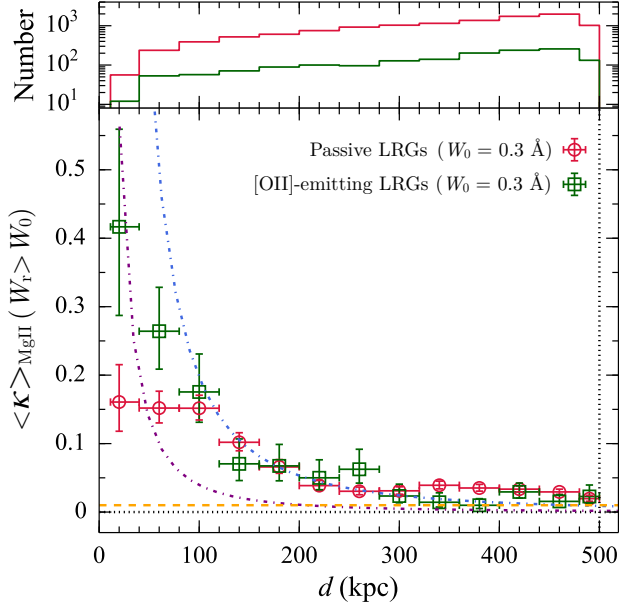


Figure 5. Mean incidence (or covering fraction) of Mg II absorbing gas $\langle \kappa \rangle_{\text{Mg II}}$ versus projected distance d for passive and [O II]-emitting LRGs. At the top, we show the number of LRGs that were considered in computing $\langle \kappa \rangle_{\text{Mg II}}$ for each projected distance bin. We adopt the LRG sample with sufficiently high S/N background QSO spectra available for detecting Mg II absorbers as weak as $W_0 = 0.3 \text{ \AA}$, and a bin size of 40 kpc. The horizontal bars mark the full range of projected distance within each bin and vertical error bars represent the 68% confidence intervals in the estimated gas covering fraction. The vertical dotted line indicates the virial radius of a typical LRG halo. We estimate the contribution due to random background absorbers that coincidentally occur within a velocity difference of $\Delta v = \pm 1000 \text{ km s}^{-1}$ from the redshifts of the LRGs (orange dashed line; see Section 3.3 for details). The blue and purple dash-dotted curves indicate the expected maximum contributions to the observed incidence of $W_r(2796) \geq 0.3 \text{ \AA}$ absorbers from all and blue satellite galaxies, respectively (see Section 4.2 for details).

fraction of $\langle \kappa \rangle_{\text{Mg II}} \approx 5\%$ at $d < 500$ kpc. In addition, $\langle \kappa \rangle_{\text{Mg II}}$ remains flat at $\langle \kappa \rangle_{\text{Mg II}} = 15\%$ at $d \lesssim 120$ kpc from passive LRGs, while it increases steadily with decreasing d from [O II]-emitting LRGs. Beyond $d \approx 120$ kpc, both passive and [O II]-emitting LRGs show consistent $\langle \kappa \rangle_{\text{Mg II}}$ to within measurement uncertainties, which gradually declines and merges into the background at $d > 300$ kpc.

Recall the finding of Chen & Tinker (2008) that typical L_* galaxies possess extended Mg II absorbing gas with an empirical gaseous radius of $R_{\text{gas}} = 130 (L_B/L_{B*})^{0.35 \pm 0.05}$ kpc. For a mean rest-frame B -band magnitude of $M_B = -22.0$ of the LRGs, corresponding to $3.6 L_*$ for $M_{B*} = -20.6$ from Cool et al. (2012), we infer $R_{\text{gas}} \approx 206$ kpc and find a mean covering fraction of $\langle \kappa \rangle_{\text{Mg II}} = 14^{+2.0}_{-0.4}\%$ at $d < R_{\text{gas}}$ from [O II]-emitting LRGs and $\langle \kappa \rangle_{\text{Mg II}} = 11^{+1.0}_{-0.2}\%$ at $d < R_{\text{gas}}$ from passive LRGs. The covering fraction is significantly smaller than what is measured for both red and blue $L_*/\text{sub-}L_*$ galaxies at $\langle \kappa \rangle_{\text{Mg II}} = (70 \pm 10)\%$ (Chen et al. 2010a), confirming

that the incidence of cool gas declines steeply with increasing halo mass for halos of $M_h \gtrsim 10^{12} M_\odot$.

While such declining trend is expected in theoretical models that attribute the observed Mg II absorbers to infalling gas from either thermally unstable hot halos or the intergalactic medium (IGM) (e.g., Maller & Bullock 2004; Kereš et al. 2009), the large clustering amplitudes found for Mg II absorbers (e.g., Bouché et al. 2006; Lundgren et al. 2009; Gauthier et al. 2009) also indicate that the incidence and covering fraction of Mg II absorbing gas is non-zero in high-mass halos (e.g., Tinker & Chen 2008). Indeed, our study based on an unprecedentedly large LRG–QSO pairs has led to a definitive detection of chemically-enriched cool gas around quiescent galaxies at a level that conclusively rules out zero covering fraction.

To better understand the origin of chemically-enriched cool gas in predominantly quiescent halos, we examine the spatial distribution of Mg II absorbing gas relative to the orientation of the host LRGs. This is motivated by the expectations that star formation driven outflows are likely to proceed along the minor (spin) axis of a disk galaxy and that accretion is likely to proceed along the major axis. The former has been seen by a number of previous studies (e.g., Bordoloi et al. 2011) but is an unlikely scenario for explaining the Mg II absorbers found around LRGs due to the observed low SFR. At the same time, it has been shown both in simulations and in observations that elliptical galaxies preferentially have their major axes aligned with the filamentary structures (e.g., Aragón-Calvo et al. 2007; Tempel et al. 2013), where accretion of intergalactic gas and satellites originates (e.g., Faucher-Giguère & Kereš 2011; Fumagalli et al. 2011; Tempel et al. 2015).

3.4 Angular Distribution of Mg II Absorption Relative to Galaxy Major Axis

To examine the azimuthal dependence of $\langle \kappa \rangle_{\text{Mg II}}$, we make use of the position angle (P.A.) and ellipticity (e) measurements, and associated measurement uncertainties, of each galaxy from the SDSS database. We refer the readers to Stoughton et al. (2002) for details on the SDSS image processing algorithm. Briefly, the position angle and ellipticity of each LRG were determined based on a two-dimensional surface brightness profile fit of a deVaucouleurs model to individual SDSS images. Uncertainties in the best-fit parameters depend on a combination of factors including the depth of the images and the size of the galaxy relative to the size of the point spread function of the image. For LRGs at $z = 0.4 - 0.7$, SDSS r - and i -bands serve as the most sensitive bandpasses for recording their surface brightness profiles. We define the azimuthal angle Φ of each QSO-LRG pair as the angle that extends from the observed major axis of the LRG to the location of the background QSO sightline. Following this definition, a QSO sightline that occurs along the major axis of the galaxy has $\Phi = 0^\circ$ and a QSO that occurs along the minor axis has $\Phi = 90^\circ$.

To ensure high confidence in the results of our azimuthal dependence investigation, we first consider only LRGs that show consistent measurements in both P.A. and e from SDSS r - and i -band imaging data. In addition, we restrict our sample for this study to those LRGs with a mea-

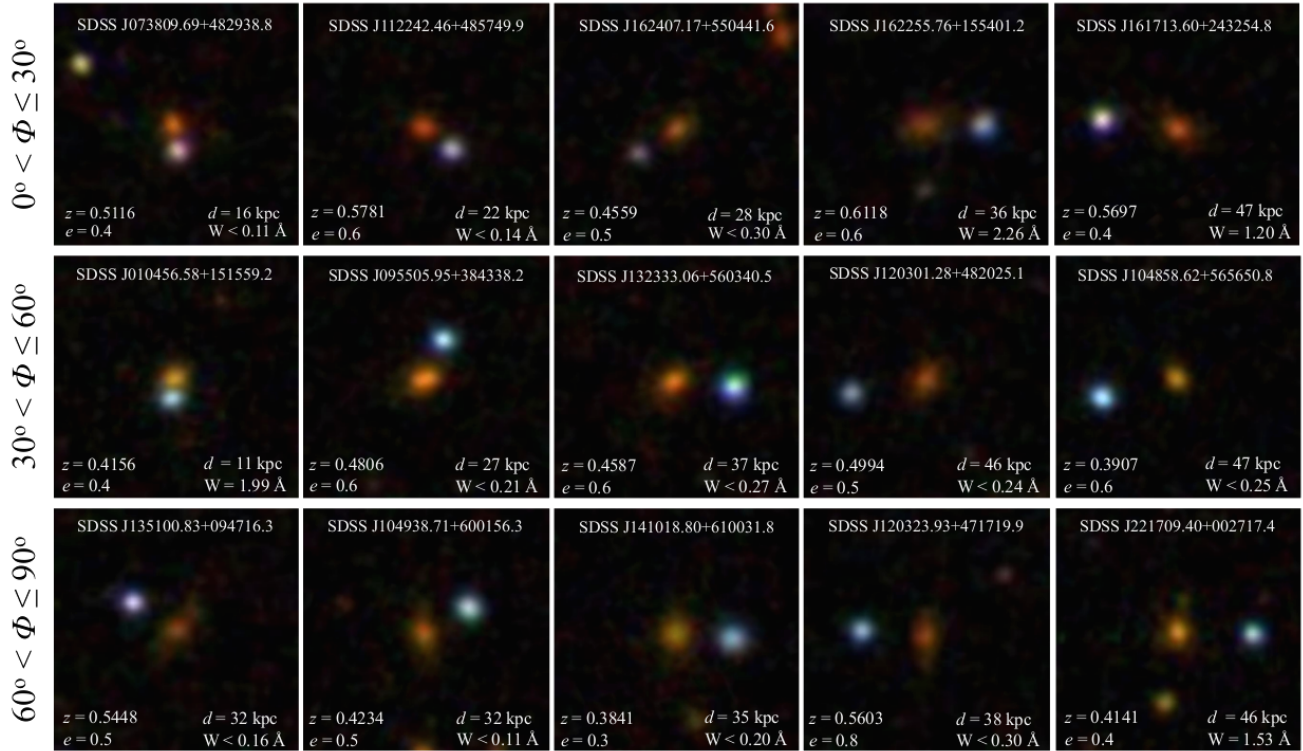


Figure 6. Images of 15 LRG-QSO pairs with $d < 50$ kpc to demonstrate visually that the accuracy of ellipticity (e) and azimuthal angle (Φ) measurements from SDSS is sufficient for the subsequent Φ -dependence study. Each panel is 150 kpc on a side. The LRG is placed at the center and the QSO appears as a blue compact source near the LRG. The projected distance of each LRG is shown in the lower-right corner together with the observed constraint for associated Mg II absorbers (measurement or $2\text{-}\sigma$ upper limits). The redshift and ellipticity of the LRG are included in the lower-left corner. The top, middle, and bottom rows display examples of LRGs with consistent measurements of Φ from their r - and i -band images in the range of $0^\circ < \Phi \leq 30^\circ$, $30^\circ < \Phi \leq 60^\circ$, and $60^\circ < \Phi \leq 90^\circ$, respectively.

sured ellipticity consistently greater than $e = 0.2$ in both r - and i -bands. This criterion removes 2545 LRGs from the total sample of 13330 LRGs. We then divide the remaining QSO-LRG pairs into different bins in Φ . The bin size is chosen to be larger than the uncertainties in Φ , which are evaluated based on the consistency of P.A. measurements from r - and i -band images. We find a typical error of $< 10^\circ$ for the P.A., and selected a bin size of $\Delta\Phi = 30^\circ$. In Figure 6, we show 15 (out of 70 total) LRG-QSO pairs with $d < 50$ kpc to illustrate typical cases with azimuthal angle falling in three bins: $0^\circ < \Phi \leq 30^\circ$ (top panels), $30^\circ < \Phi \leq 60^\circ$ (middle panels), and $60^\circ < \Phi \leq 90^\circ$ (bottom panels). A visual inspection of Figure 6 confirms that measurements of Φ are sufficiently accurate for the adopted bin size in Φ .

In Figure 7, we show $\langle\kappa\rangle_{\text{Mg II}}$ as a function of Φ in different projected distance bins. Passive LRGs are shown in the left panel and [O II]-emitting LRGs are shown in the right panel. At $d \geq 50$ kpc, we find no strong dependence of $\langle\kappa\rangle_{\text{Mg II}}$ on Φ for either passive or [O II]-emitting LRGs. While there is little azimuthal angle preference for passive LRGs at $d \leq 50$ kpc, we find a modest ($\approx 50\%$) enhancement of Mg II absorption closer to the major axis ($\Phi \lesssim 60^\circ$) of [O II]-emitting LRGs. The excess of Mg II covering fraction decreases with increasing Φ and becomes consistent with that of passive LRGs at $\Phi > 60^\circ$. Recall that we have shown in Figure 5 the overall enhancement of covering fraction for

[O II]-emitting LRGs as compared to passive LRGs at $d \leq 80$ kpc. We find this difference in $\langle\kappa\rangle_{\text{Mg II}}$ is likely driven by an elevated incidence of Mg II absorbing gas at small azimuthal angles. The difference in the observed azimuthal dependence between [O II]-emitting and passive LRGs suggests that additional sources are responsible for the observed Mg II absorbing gas around [O II]-emitting galaxies. We will discuss this further in § 4.4 below.

4 DISCUSSION

Our study based on an unprecedentedly large sample of LRG-QSO pairs has led to a definitive detection of chemically-enriched cool gas around massive, quiescent galaxies at a level that conclusively rules out zero covering fraction of cool gas in these massive halos. The result is based on a survey of 37621 LRG-QSO pairs with projected separations of < 500 kpc, which yielded a sample of 13330 LRGs at $z \approx 0.4\text{--}0.7$ with sensitive background QSO spectra available for constraining the presence/absence of Mg II absorbers of $W_r(2796) \geq 0.3 \text{ \AA}$. Roughly 13% of these LRGs exhibit [O II] emission features that indicate a mean on-going star formation rate of $\text{SFR} \sim 0.8 M_\odot \text{ yr}^{-1}$ among otherwise old (age $\gtrsim 1$ Gyr) stellar populations. The remaining 87% of the LRGs exhibit no trace of on-going star formation with $2\text{-}\sigma$ upper limit of $\text{SFR} \lesssim 0.1 M_\odot \text{ yr}^{-1}$ and a

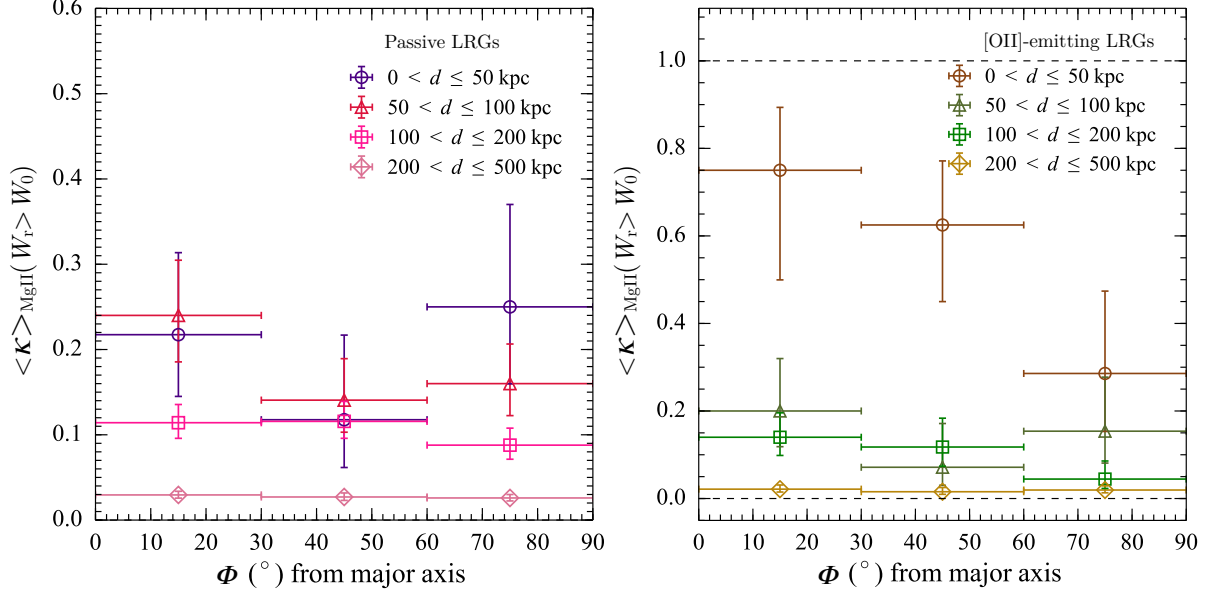


Figure 7. Dependence of $\langle \kappa \rangle_{\text{Mg II}}$ on the azimuthal angle in different projected distance intervals for passive (*left*) and [O II]-emitting LRGs (*right*). The azimuthal angle is measured with respect to the major axis of the LRGs. Circles represent LRGs within projected distance d of $0 < d \leq 50$ kpc from a background QSO sightline, triangles represent $50 < d \leq 100$ kpc, squares represent $100 < d \leq 200$ kpc and diamonds represent $200 < d \leq 500$ kpc. The horizontal error bars show the full range in projected distance of each bin and vertical error bars represent the 68% confidence interval. Note that we have zoomed in along the y-axis in the left panel in order to better illustrate the range of observed $\langle \kappa \rangle_{\text{Mg II}}$ for the passive galaxies.

mean stellar age $\gtrsim 1$ Gyr. Both passive and [O II]-emitting LRGs share a very similar distribution in stellar mass with a mean of $\langle \log(M_*/M_\odot) \rangle \approx 11.4$ and a dispersion of 0.2 dex.

Strong Mg II absorbers are found at $d < 500$ kpc from both passive and [O II]-emitting LRGs with a mean gas covering fraction of $\langle \kappa \rangle_{\text{Mg II}} \approx 5\%$. While strong Mg II absorbers continue to be found at distances as large as the virial radius in the halos, the mean gas covering fraction declines rapidly with increasing d . The mean covering fraction of Mg II absorbers increases to $\langle \kappa \rangle_{\text{Mg II}} \approx 11 - 14\%$ within the fiducial gaseous radius $R_{\text{gas}} \approx 200$ kpc inferred for super- L_* galaxies from Chen & Tinker (2008), and continues to increase to $\langle \kappa \rangle_{\text{Mg II}} \gtrsim 15\%$ at smaller radii at $d \lesssim 120$ kpc. At $d < 80$ kpc, the observed gas covering fraction around [O II]-emitting LRGs is twice of what is seen around passive LRGs. No clear dependence on stellar mass is found for the observed Mg II absorption properties. These results confirm and significantly improve upon earlier reports for the presence of cool halo gas around LRGs by Gauthier et al. (2009, 2010).

In addition to constraining the incidence and covering fraction of Mg II absorbers in LRG halos, we have also further examined the kinematic and spatial distribution of Mg II absorbing gas relative to the galaxies. An intriguing finding is that the observed velocity dispersion of Mg II absorbing gas relative to either passive or [O II]-emitting LRGs is merely 60% of what is expected from virial motion in these massive halos (§ 3.2 & Figure 4), which is similar to what has been previously reported by Zhu et al. (2014). Furthermore, we have also investigated possible azimuthal dependence in the incidence and covering fraction of Mg II absorbers of

$W_r(2796) \geq 0.3 \text{ \AA}$. While no apparent trend is seen for passive LRGs at all radii, a surprising result is a modest enhancement in the gas covering fraction along the major axis of [O II]-emitting LRGs at $d < 50$ kpc (§ 3.3 & Figure 7). This is opposite of what was found for star-forming galaxies at $z \approx 0.7$ by Bordoloi et al. (2011).

The observed suppression in the velocity dispersion of Mg II absorbing gas around both passive and [O II]-emitting LRGs, together with an elevated Mg II gas covering fraction along the major axis of [O II]-emitting LRGs at $d < 50$ kpc, provides important insights into the origin of the observed chemically-enriched cool gas in LRG halos. Here we discuss whether/how different scenarios are compatible with these findings.

4.1 Hot Winds due to AGN or Evolved Stars

We first consider the scenario of hot winds driven by either evolved stars or AGN as a primary driver to pollute the LRG halos with heavy elements. While the observed low SFR and a predominantly old stellar population rules out a strong influence of young starburst driven winds on the halo gas of LRGs, the influence of AGN feedback can be dominant (e.g., McNamara & Nulsen 2007, 2012). In particular, radio-mode feedback has been invoked in galaxy formation models to suppress star formation in massive halos (e.g., Croton et al. 2006). In addition, a cross-comparison between SDSS LRGs and FIRST radio sources has identified $\approx 3\%$ of the LRGs hosting radio-loud AGN (e.g., Sadler et al. 2007), and efforts in search of fainter radio emission in the remaining LRGs based on median stacks of FIRST images have continued to uncover radio signals at a level of

a few $\times 10 \mu\text{Jy}$ (e.g., Hodge et al. 2008, 2009). Continuing detections of radio fluxes in LRGs as the sensitivities of the searches improve suggests that nearly all LRGs harbor an active nucleus but with varying radio power.

The presence of AGN in these LRGs also provides a natural explanation for the observed high $[\text{N II}]/\text{H}\alpha$ emission ratio in the stacked LRG spectra presented in Figure 2 (e.g., Johnston et al. 2008; Hodge et al. 2008). It is therefore reasonable to expect that the LRG halos are being regulated by AGN winds that provide an additional heating source.

In contrast, the observed low $[\text{O III}]/[\text{O II}]$ ratios in $[\text{O II}]$ -emitting LRGs resemble the spectra of LINER-like galaxies, rather than star-forming regions or Seyfert galaxies (e.g., Yan et al. 2006). The observed LINER-like spectra can be explained by photo-ionization due to post-asymptotic giant branch (post-AGB) stars (e.g., Binette et al. 1994). This is motivated by recent observations that have uncovered spatially extended LINER signals in passive red galaxies with a surface brightness profile shallower than r^{-2} (e.g., Sarzi et al. 2006, 2010; Yan & Blanton 2012; Singh et al. 2013). The shallow, extended surface brightness profiles are inconsistent with the gas being ionized by a central point source, but indicate a spatially distributed ionizing source.

However, connecting the observed cool gas revealed by Mg II absorption with AGN/stellar winds remains challenging, particularly because of the suppressed velocity dispersion of Mg II absorbing gas relative to the LRGs. Recall from Figure 4 and § 3.2 that the observed velocity dispersion of Mg II absorbing gas relative to either passive or $[\text{O II}]$ -emitting LRGs is merely 60% of what is expected from virial motion in these massive halos. One would expect that including AGN/stellar winds would further stir up halo gas motion (e.g., Johnson et al. 2015), increasing/maintaining the velocity dispersion rather than suppressing it. We therefore find this scenario to be an unlikely explanation of the observed Mg II absorbers in LRG halos.

4.2 Environmental Effects

Next, we consider possible environmental effects that may contribute to the observed Mg II absorbers in LRGs halos. The large mean bias found for LRGs (e.g., Padmanabhan et al. 2007; Gauthier et al. 2009) indicate not only that these galaxies reside in massive halos but also that they reside in relatively more overdense environment. First, we consider gas-rich satellites that could contribute to some fraction of the observed Mg II absorbers, if the satellites can retain a significant fraction of their gas.

Under the assumption that the gas content of satellite galaxies remains intact in LRG halos, we estimate the expected *maximal* contribution to the covering fraction of Mg II absorbing gas from these satellites. Following Gauthier et al. (2010), we first adopt the subhalo mass function from Tinker & Wetzel (2010). The subhalo mass is defined as the mass at the time of accretion and therefore is suitable for calculating the intact gaseous halo. Next, we adopt the gaseous radius at $W_r(2796) \geq 0.3 \text{ \AA}$, R_{gas} , and a mean covering fraction of κ_{gas} within R_{gas} for a given subhalo mass (M_{sub}) from Tinker & Chen (2008). Then we adopt the surface mass density profile of satellite galaxies from Budzynski et al. (2012), which is characterized by a projected Navarro–Frenk–White profile with a concentration

parameter $\langle c \rangle \equiv \langle r_{\text{vir}}/r_s \rangle \approx 2.6$ from , where r_{vir} is the virial radius and r_s is the scale radius. The best-fit concentration parameter was found to be nearly independent of mass and a factor of two lower than what is found for the dark matter halo. Given a host halo mass M_{host} (in this case, $10^{13.4} M_{\odot}$), the covering fraction of subhalos as a function of projected distance d is then computed according to

$$\kappa_{\text{sub}}(M_{\text{host}}, d) = \frac{f(d, M_{\text{host}})}{\pi R_{\text{vir}}^2(M_{\text{host}})} \int dM_{\text{sub}} n(M_{\text{sub}}|M_{\text{host}}) \times \pi R_{\text{g}}^2(M_{\text{sub}}, W_r = 0.3) \kappa_{\text{g}}(M_{\text{sub}}) \quad (3)$$

where $f(d, M_{\text{host}})$ is the probability of having subhalos at d and $n(M_{\text{sub}}|M_{\text{host}})$ is the subhalo mass function from Tinker & Wetzel (2010). The estimated, *maximal* covering fraction of Mg II absorbers versus projected distance is shown in Figure 5 (blue dashed-dotted curve). Our calculation demonstrates that if satellite galaxies can retain their gas, then they can fully account for the observed Mg II covering fraction.

Many studies have shown that galaxies in denser environments tend to have a higher fraction of red galaxies at $z \lesssim 1$ (e.g., Gerke et al. 2007; Skibba 2009; Smith et al. 2012; Kovač et al. 2014), indicating that the star formation has been shut down either due to gas exhaustion or removal by environmental effects. Quantitatively speaking, the red satellite fraction decreases from $\sim 80\%$ at projected radius $\lesssim 100$ kpc from L_* satellite galaxies to $\sim 70\%$ at about the virial radius (e.g., Hansen et al. 2009; Prescott et al. 2011). Here we consider only L_* halos because they are expected to be the dominant contributor to the Mg II covering fraction from a halo occupation analysis (Tinker & Chen 2008, 2010). If we further restrict the blue (and therefore gas rich) satellite fraction to be 20% and assume that these blue satellites can retain their gaseous halos, then the expected, maximal blue satellite contribution is shown as the purple dashed-dotted curve in Figure 5. We find that blue satellites alone cannot account for the observed 15% covering fraction of Mg II absorbing gas at $d \approx 100$ kpc from the LRGs but could be a main contributor to the incidence of gas at $d \lesssim 40$ kpc.

Incidentally, the spatial distribution of satellites is found to be aligned with the major axis of the brightest galaxies in groups (e.g., Yang et al. 2006; Donoso et al. 2006; Wang et al. 2008). While the effect is more subtle for blue satellites than red satellites, Yang et al. (2006) found that blue satellites along the major axis are $\sim 25\%$ more abundant than along the minor axis. This is qualitatively consistent with the trend found in the azimuthal dependence of $\langle \kappa \rangle_{\text{Mg II}}$ in Figure 7.

However, ram pressure and tidal stripping are expected to be effective in removing gas from satellite galaxies (e.g., Gunn & Gott 1972; Balogh et al. 2000; Kawata & Mulchaey 2008). These dynamical processes should redistribute chemically-enriched cool ISM and halo gas of blue satellites to larger distances, consequently further suppressing the incidence of cool gas due to satellites in inner LRG halos. This expectation is qualitatively consistent with the observed flat distribution of $W_r(2796)$ versus projected distance. The presence of strong Mg II absorbers out to the virial radius also suggests that these LRGs possibly reside in a group/cluster environment (e.g., Whiting et al. 2006;

Kacprzak et al. 2010; Gauthier 2013). A remaining caveat is to explain the suppressed velocity dispersion of Mg II gas around LRGs. In summary, if red satellites have their gas removed, then satellites do not explain the Mg II covering fraction, unless the cool gas survives in the halo after removal.

4.3 Condensing Cool Clouds due to Thermal Instabilities

Next, we consider a third possibility of the observed Mg II absorbers arising in cool clouds that are condensing out of thermally-unstable hot halos around the LRGs. A two-phase medium was first considered by Mo & Miralda-Escudé (1996) for explaining the observed QSO absorption systems as cool clouds in pressure equilibrium with the hot halo, which was subsequently expanded by Maller & Bullock (2004) to include multi-phase cooling for understanding the formation and survival of high-velocity clouds found in the Milky Way halo. These earlier analytic models have relied on a simple hypothesis that thermal instabilities would develop if the cooling time (t_{cool}) is comparable to or smaller than the dynamical time (t_{ff}) of the gas. However, recent numerical simulations have provided more detailed insights into the process of forming a multi-phase medium (e.g., McCourt et al. 2012; Sharma et al. 2012). It has been shown that, in fact, a multi-phase medium starts to develop when the cooling time is 3 – 10 times the free-fall time (Sharma et al. 2012). Indeed, multi-phase gas has been observed in clusters and nearby ellipticals with extended nebular emission from relatively cool gas embedded in hot, x-ray emitting halos (e.g., Werner et al. 2014), and the gas in those cooling clusters and ellipticals is found to satisfy the criterion of $t_{\text{cool}}/t_{\text{ff}} \lesssim 10$ (Voit et al. 2015a,b).

Direct observations to distinguish between the presence and absence of a multi-phase medium around the LRGs in our sample are beyond the reach of current-generation facilities. Nevertheless, we expect that these LRGs to be surrounded by a hot halo, given that the Sunyaev-Zel'dovich decrement in the cosmic microwave background radiation has been detected in stacks of 148 GHz maps of higher-mass LRGs with $M_h \sim 10^{14} M_{\odot}$ (Hand et al. 2011). Under the multi-phase cooling hypothesis, we expect to see cool clouds form within a cooling radius R_c where thermal instabilities occur. Observations of $z \approx 0.5$ galaxy clusters indicate that R_c occurs between 1/3 and 2/3 of the virial radius (e.g., Voit et al. 2015a). For LRGs in our sample, this corresponds to a cooling radius of 160 – 320 kpc. Condensing cool clouds may explain the rapid decline in $\langle \kappa \rangle_{\text{Mg II}}$ at $d > 120$ kpc, although they cannot explain the strong Mg II absorbers detected in the outer halos near the virial radius.

A natural expectation for condensed cool clouds traveling through a hot halo is a ram-pressure drag force that would slow down the cloud motion. If the clouds are not sufficiently massive, then we expect to observe significant deceleration. This provides a physical model for explaining the observed suppression of velocity dispersion between Mg II absorbers and LRGs in Figure 4 and places a maximum limit on the cloud mass. Following Maller & Bullock (2004), we compute the mass limit using their Equation (40),

$$m_{\text{cl}} \approx 5.1 \times 10^4 M_{\odot} T_6^{-3/8} (\Lambda_z t_8)^{1/2}, \quad (4)$$

where T_6 is the halo gas temperature in units of 10^6 K, Λ_z is the cooling parameter that varies with the gas metallicity Z_g and $t_8 = t_f(c_h)/8$ Gyr is the halo formation time that depends on the halo concentration c_h . We estimate $T \sim 6 \times 10^6$ K assuming isothermal hot gas for the LRG halos, and $t_8 \sim 8.9$ Gyr using $c_h \sim 10$ from the halo mass–concentration relation (e.g., Mandelbaum et al. 2008). We find $m_{\text{cl}} = 2.8 \times 10^4 M_{\odot}$ for a gas metallicity of $Z_g = 0.1 Z_{\odot}$, and $m_{\text{cl}} = 4.9 \times 10^4 M_{\odot}$ for $Z_g = Z_{\odot}$. Note that for clouds of this low mass, it would require $n_{\text{cl}} \sim 20$ of these to make up the total observed absorption strength per sightline (see Chen et al. 2010a). This is consistent with the previous finding that strong Mg II absorbers identified in moderate-resolution spectra are routinely resolved into multiple components in high-resolution spectra, with $W_r(2796)$ roughly proportional to the number of components in the system (e.g., Petitjean & Bergeron 1990 ; Prochter et al. 2006). However, the inferred maximum cloud mass for the ram-pressure drag to be dominant also indicates that the clouds would be likely to evaporate due to thermal conduction of the hot halo in $\tau_{\text{evap}} \sim 100$ Myr from Equation (35) of Maller & Bullock (2004). Taking into account a prolonged infall time of $\tau_{\text{infall}} \approx 400 - 600$ Myr for clouds formed at R_c from Equation (43) of Maller & Bullock (2004) due to ram-pressure drag, we conclude that only clouds formed at $d < 100$ kpc will be able to reach the center.

4.4 Accretion along Filaments

Recent simulations have shown that galaxies of all mass acquire most of their baryonic mass through filamentary accretion from the IGM (e.g., Kereš et al. 2009; Stewart et al. 2011). In these narrow, dense streams, the cool gas would never be shock heated to the virial temperature and can penetrate deep toward the central regions of dark matter halos. Given that LRGs reside in overdense regions, a sizable fraction of central LRGs may be at the focus of cold accretion through filaments. In the cold accretion scenario, hydrodynamical simulations show that HI gas has a roughly constant covering fraction at radii $\lesssim 100$ kpc at $z \approx 2.5$ (e.g., Dekel et al. 2009). It is intriguing because the behavior is in a broad agreement with the observed covering fraction within ~ 100 kpc in our passive LRG sample. However, the cold-mode accretion is expected to be efficient only for galaxies at high redshifts $z \gtrsim 2$ (e.g., Dekel et al. 2009) or low-mass galaxies at lower redshifts. At $z < 1$, the mechanism might not be effective in high-mass halos, and cold filaments might be truncated or disrupted before reaching the center (e.g., Kereš et al. 2009).

In addition to intergalactic gas, satellite accretion is also expected to proceed along filaments based on the preferential alignment of satellite galaxies along the major axis of massive central galaxies (e.g., Yang et al. 2006) and the parallel alignment of the major axis of galaxies and surrounding filaments (e.g., Tempel et al. 2013, 2015). If the observed Mg II absorbers arise in accreted satellites along a more confined large-scale filament, then we can simultaneously explain the enhanced $\langle \kappa \rangle_{\text{Mg II}}$ along the major axis of [O II]-emitting LRGs at $d < 50$ kpc and the observed reduced velocity dispersion relative to what is expected for virialized gas in massive halos.

5 SUMMARY AND CONCLUSIONS

We study the chemically-enriched cool gas content in massive halos based on a survey of Mg II absorbers associated with 37621 LRGs in the spectra of background QSOs. Mg II absorption is detected around both passive and [O II]-emitting LRGs. The covering fraction of Mg II gas is higher around [O II]-emitting LRGs inside 100 kpc; the covering fraction in both passive and [O II]-emitting LRGs declines rapidly with radius. Both Mg II-absorbing and non-absorbing LRGs show comparably old stellar populations. There is a weak azimuthal dependence of absorption: [O II]-emitting LRGs show more absorption along the major axis. This trend is only significant within 50 kpc. The velocity dispersion of Mg II relative to the LRGs is less than expected for LRG halo masses in both types of galaxy.

We find that the observed Mg II absorbers in the vicinities of LRGs are best-explained by a combination of cool clouds formed through thermal instabilities in LRG halos and satellite accretion through filaments that are preferentially aligned with the major axis of the LRGs. While AGN are likely present in nearly all of the LRGs in our sample, the suppressed velocity dispersion found for the Mg II absorbing gas makes AGN winds an unlikely contributor. We expect that follow-up analysis of available imaging data around the LRGs will provide the necessary test for the accreting satellite scenario.

ACKNOWLEDGMENTS

It is a pleasure to thank Jenny Greene, Hung-Jin Huang, Cameron Liang, Michael Rauch, and Mark Voit for helpful discussions on the interpretations of our main findings. We thank an anonymous referee for constructive comments that helped improve the presentation of the paper. HWC acknowledges the Aspen Center for Physics, which is supported by National Science Foundation grant PHY-1066293, and the organizers of the workshop on the “physics of accretion and feedback in the circumgalactic medium” for a productive visit in June 2015, during which components of the work presented were accomplished. We are grateful to the SDSS collaboration for producing and maintaining the SDSS public data archive. Funding for SDSS-III has been provided by the Alfred P. Sloan Foundation, the Participating Institutions, the National Science Foundation, and the U.S. Department of Energy Office of Science. The SDSS-III web site is <http://www.sdss3.org/>.

SDSS-III is managed by the Astrophysical Research Consortium for the Participating Institutions of the SDSS-III Collaboration including the University of Arizona, the Brazilian Participation Group, Brookhaven National Laboratory, Carnegie Mellon University, University of Florida, the French Participation Group, the German Participation Group, Harvard University, the Instituto de Astrofísica de Canarias, the Michigan State/Notre Dame/JINA Participation Group, Johns Hopkins University, Lawrence Berkeley National Laboratory, Max Planck Institute for Astrophysics, Max Planck Institute for Extraterrestrial Physics, New Mexico State University, New York University, Ohio State University, Pennsylvania State University, University of Portsmouth, Princeton University, the Spanish Participation Group, University of Tokyo, University of Utah,

Vanderbilt University, University of Virginia, University of Washington, and Yale University.

REFERENCES

- Agertz O., Teyssier R., Moore B., 2009, MNRAS, 397, L64
 Alam S., Albareti F. D., Allende Prieto C., Anders F., Anderson S. F., Andrews B. H., Armengaud E., Aubourg É., Bailey S., Bautista J. E., et al., 2015, ApJS, 219, 12
 Aragón-Calvo M. A., van de Weygaert R., Jones B. J. T., van der Hulst J. M., 2007, ApJ, 655, L5
 Balogh M. L., Morris S. L., Yee H. K. C., Carlberg R. G., Ellingson E., 1999, ApJ, 527, 54
 Balogh M. L., Navarro J. F., Morris S. L., 2000, ApJ, 540, 113
 Bergeron J., Stasińska G., 1986, A&A, 169, 1
 Binette, L., Magris, C. G., Stasińska, G., Bruzual, A. G., 1994, A&A, 292, 13
 Blake C., Collister A., Lahav O., 2008, MNRAS, 385, 1257
 Blanton M. R., Roweis S., 2007, AJ, 133, 734
 Bolton A. S., Brownstein J. R., Kochanek C. S., et al. 2012, ApJ, 757, 82
 Bordoloi R., Lilly S. J., Knobel C., et al. 2011, ApJ, 743, 10
 Bouché N., Murphy M. T., Péroux, C., Csabai I., Wild V., 2006, MNRAS, 371, 495
 Bowen D. V., Blades J. C., Pettini M., 1995, ApJ, 448, 634
 Budzynski J. M., Kuposov S. E., McCarthy I. G., McGee S. L., Belokurov V., 2012, MNRAS, 423, 104
 Charlton J. C., Ding J., Zonak S. G., Churchill C. W., Bond N. A., Rigby J. R., 2003, ApJ, 589, 111
 Chen H.-W., Tinker J. L., 2008, ApJ, 687, 745
 Chen H.-W., Helsby J. E., Gauthier J.-R., Shectman S. A., Thompson I. B., Tinker J. L., 2010a, ApJ, 714, 1521
 Chen, H.-W., Wild, V., Tinker, J. L., Gauthier, J.-R., Helsby, J. E., Shectman, S. A., & Thompson, I. B. 2010b, ApJ, 724, L176
 Coleman G. D., Wu C.-C., Weedman D. W., 1980, ApJS, 43, 393
 Cool, R. J., Eisenstein, D. J., Kochanek, C. S. et al. (2012), ApJ, 748, 10
 Croton D. J., Springel V., White S. D. M., De Lucia G., Frenk C. S., Gao L., Jenkins A., Kauffmann G., Navarro J. F., Yoshida N., 2006, MNRAS, 365, 11
 Dawson K. S., Schlegel D. J., Ahn C. P., et al. 2013, AJ, 145, 10
 Dekel A., Birnboim Y., Engel G., Freundlich J., Goerdt T., Mumcuoglu M., Neistein E., Pichon C., Teyssier R., Zinger E., 2009, Nature, 457, 451
 Donoso E., O’Mill A., Lambas D. G., 2006, MNRAS, 369, 479
 Eisenstein D. J., Annis J., Gunn J. E., et al. 2001, AJ, 122, 2267
 Eisenstein D. J., Weinberg D. H., et al. 2011, AJ, 142, 72
 Faucher-Giguère C.-A., Kereš D., 2011, MNRAS, 412, L118
 Fumagalli M., Prochaska J. X., Kasen D., Dekel A., Ceverino D., Primack J. R., 2011, MNRAS, 418, 1796
 Gauthier J.-R., Chen H.-W., Tinker J. L., 2009, ApJ, 702, 50
 —, 2010, ApJ, 716, 1263
 Gauthier J.-R., Chen H.-W., 2011, MNRAS, 418, 2730

- Gauthier J.-R., 2013, *MNRAS*, 432, 1444
- Gerke B. F., Newman J. A., Faber S. M., Cooper M. C., Croton D. J., Davis M., Willmer C. N. A., Yan R., Coil A. L., Guhathakurta P., Koo D. C., Weiner B. J., 2007, *MNRAS*, 376, 1425
- Gunn J. E., Gott III J. R., 1972, *ApJ*, 176, 1
- Hand N., Appel J. W., Battaglia N., et al. 2011, *ApJ*, 736, 39
- Hansen S. M., Sheldon E. S., Wechsler R. H., Koester B. P., 2009, *ApJ*, 699, 1333
- Hodge J. A., Becker R. H., White R. L., de Vries W. H., 2008, *AJ*, 136, 1097
- Hodge J. A., Zeimann G. R., Becker R. H., White R. L., 2009, *AJ*, 138, 900
- Johnson S. D., Chen H.-W., Mulchaey J. S., 2015, *MNRAS*, 452, 2553
- Johnston H. M., Sadler E. M., Cannon R., Croom S. M., Ross N. P., Schneider D. P., 2008, *MNRAS*, 384, 692
- Kacprzak G. G., Murphy M. T., Churchill C. W., 2010, *MNRAS*, 406, 445
- Kauffmann G., Heckman T. M., White S. D. M., et al. 2003, *MNRAS*, 341, 33
- Kawata D., Mulchaey J. S., 2008, *ApJL*, 672, L103
- Kennicutt Jr. R. C., Evans N. J. 2012, *ARA&A*, 50, 531
- Kereš D., Katz N., Fardal M., Davé R., Weinberg D. H., 2009, *MNRAS*, 395, 160
- Kovač K., Lilly S. J., Knobel C., et al. 2014, *MNRAS*, 438, 717
- Lundgren B. F., Brunner R. J., York D. G., Ross A. J., Quashnock J. M., Myers A. D., Schneider D. P., Al Sayyad Y., Bahcall N., 2009, *ApJ*, 698, 819
- Maller A. H., Bullock J. S., 2004, *MNRAS*, 355, 694
- Mandelbaum R., Seljak U., Hirata C. M., 2008, *JCAP*, 8, 6
- McCourt M., Sharma P., Quataert E., Parrish I. J., 2012, *MNRAS*, 419, 3319
- McNamara B., Nulsen P. E. J., 2007, *ARA&A*, 45, 117
- McNamara B., Nulsen P. E. J., 2012, *NJPh*, 14, 55023
- Mo H. J., Miralda-Escude J., 1996, *ApJ*, 469, 589
- Murray N., Ménard B., Thompson T. A., 2011, *ApJ*, 735, 66
- Nelson D., Vogelsberger M., Genel S., Sijacki D., Kereš D., Springel V., Hernquist L., 2013, *MNRAS*, 429, 3353
- Nestor D. B., Turnshek D. A., Rao S., 2005, *ApJ*, 628, 637
- Nestor D. B., Johnson B. D., Wild V., Ménard B., Turnshek D. A., Rao S., Pettini M., 2011, *MNRAS*, 412, 1559
- Petitjean P., Bergeron J., 1990, *A&A*, 231, 309
- Prochter G. E., Prochaska J. X., Burles S. M. 2006, *ApJ*, 639, 766
- Oosterloo T. A., Morganti R., Crocker A., 2010, *MNRAS*, 409, 500
- Padmanabhan N., Schlegel D. J., Seljak U., et al. 2007, *MNRAS*, 378, 852
- Prescott M., Baldry I. K., James P. A., et al. 2011, *MNRAS*, 417, 1374
- Rao S. M., Turnshek D. A., Nestor D. B., 2006, *ApJ*, 636, 610
- Roseboom I. G., Pimbblet K. A., Drinkwater M. J., et al. 2006, *MNRAS*, 373, 349
- Sadler E. M., Cannon R. D., Mauch T., et al. 2007, *MNRAS*, 381, 211
- Sarzi M., Falcón-Barroso J., Davies R. L., et al. 2006, *MNRAS*, 366, 1151
- Sarzi M., Shields J. C., Schawinski K., et al. 2010, *MNRAS*, 402, 2187
- Sharma P., McCourt M., Quataert E., Parrish I. J., 2012, *MNRAS*, 420, 3174
- Singh R., van de Ven G., Jahnke K., et al. 2013, *A&A*, 558, 43
- Skibba R. A., 2009, *MNRAS*, 392, 1467
- Smee S. A., Gunn J. E., Uomoto A., et al. 2013, *AJ*, 146, 32
- Smith R. J., Lucey J. R., Price J., Hudson M. J., Phillipps S., 2012, *MNRAS*, 419, 3167
- Steidel C. C., Dickinson M., Persson S. E., 1994, *ApJ*, 437, L75
- Steidel C. C., Dickinson M., Meyer D. M., Adelberger K. L., Sembach K. R., 1997, *ApJ*, 480, 568
- Stewart K. R., Kaufmann T., Bullock J. S., Barton E. J., Maller A. H., Diemand J., Wadsley J., 2011, *ApJL*, 735, L1
- Stoughton C., Lupton R. H., Bernardi M., et al. 2002, *AJ*, 123, 485
- Tempel E., Stoica R. S., Saar, E., 2013, *MNRAS*, 428, 1827
- Tempel E., Guo, Q., Kipper, R., Libeskind, N. I., 2015, *MNRAS*, 450, 2727
- Tinker J. L., Chen H.-W., 2008, *ApJ*, 679, 1218
- , 2010, *ApJ*, 709, 1
- Tinker J. L., Wetzel A. R., 2010, *ApJ*, 719, 88
- Tojeiro R., Percival W. J., Heavens A. F., Jimenez R., 2011, *MNRAS*, 413, 434
- Voit G. M., Donahue M., Bryan G. L., McDonald M., 2015a, *Nature*, 519, 203
- Voit G. M., Donahue M., O’Shea B. W., Bryan, G. L., Sun, M., Werner, N., 2015b, *ApJ*, 803, L21
- Wang Y., Yang X., Mo H. J., Li C., van den Bosch F. C., Fan Z., Chen X., 2008, *MNRAS*, 385, 1511
- Weiner B. J., Coil A. L., Prochaska J. X., et al. 2009, *ApJ*, 692, 187
- Werner N., Oonk J. B. R., Sun M., et al. 2014, *MNRAS*, 439, 2291
- Whiting M. T., Webster R. L., Francis P. J., 2006, *MNRAS*, 368, 341
- Worthey G., Ottaviani D. L., 1997, *ApJS*, 111, 377
- Yan R., Newman J. A., Faber S. M., Konidaris N., Koo D., Davis M., 2006, *ApJ*, 648, 281
- Yan R., Blanton M. R., 2012, *ApJ*, 747, 61
- Yang X., van den Bosch F. C., Mo H. J., Mao S., Kang X., Weinmann S. M., Guo Y., Jing Y. P., 2006, *MNRAS*, 369, 1293
- York D. G., et al. 2000, *AJ*, 120, 1579
- Zhu G., Ménard B., Bizyaev D., et al. 2014, *MNRAS*, 439, 3139